Master in Chemical Engineering

Evaluation of the Potential of Transition Metal Phosphide Catalysts in the Production of Hydrogen from Water Electrolysis

A Master's dissertation

of

Diogo Miguel Marques Abreu

Developed within the course of dissertation

Held in

INTERNATIONAL IBERIAN NANOTECHNOLOGY LABORATORY

SREC M LABORATORY OF SEPARATION AND REACTION ENGINEERING
LABORATORY OF CATALYSIS AND MATERIALS

Supervisors at FEUP: **Dra. Olívia Salomé Pinto Soares**

Professor Dr. Manuel Fernando Pereira

Supervisors at INL: **Dra. Juliana Sousa**

Dr. Yury Kolen'ko

U.PORTO
FEUP FACULDADE DE ENGENHARIA
UNIVERSIDADE DO PORTO

Departamento de Engenharia Química

October of 2018

"Difficulties are meant to rouse, not discourage.
The human spirit is to grow strong by conflict."
William Ellery Channing

Acknowledgment

I want to thank to the people that contributed to the accomplishment of this dissertation.

First, to Dra. Salomé Soares, for giving me the opportunity to realize this thesis, for the guidance and availability showed. Your cooperation was essential to the conclusion of this work.

To Professor Dr. Manuel Fernando Pereira, for selecting me for this dissertation, for the guidance, encouragement and support provided.

To Dra. Juliana Sousa, for the supervision and constant support. Thank you for all the advice, the exigence and the enormous availability in the lab.

To Dr. Yury Kolen'ko, for the guidance, cooperation and the knowledge provided. I appreciate all the encouragement, essential in the realization of this project. I also acknowledge your sympathy, which undoubtedly facilitated my integration into the INL.

To the scientists of the Nanochemistry Research Group in INL, for all the cooperation and for allowing me to be integrated into a research center of such high quality and requirement.

To Patrícia, Raquel, Carla and Natália for the incentives and collaboration provided at the Laboratory of Separation and Reaction Engineering - Laboratory of Catalysis and Materials (LSRE-LCM) of the Faculty of Engineering of the University of Porto (FEUP).

To my parents, for the support and encouragement in the fulfillment of my goals and in the accomplishment of another stage of my formation. Despite the distance, you contribute decisively to my success. Thank you for everything.

To all my friends, it was a pleasure to spend these five years with you. I appreciate the companionship and encouragement you always have given me. I certainly will never forget you.

Finally, to all the other people who somehow were involved in this thesis, here are my thanks.

This work is a result of project "AIProcMat@N2020 - Advanced Industrial Processes and Materials for a Sustainable Northern Region of Portugal 2020", with the reference NORTE-01-0145-FEDER-000006, supported by Norte Portugal Regional Operational Program (NORTE 2020), under the Portugal 2020 Partnership Agreement, through the European Regional Development Fund (ERDF) and of Project POCI-01-0145-FEDER-006984 – Associate Laboratory LSRE-LCM funded by ERDF through COMPETE2020 - Programa Operacional Competitividade e Internacionalização (POCI) – and by national funds through FCT - Fundação para a Ciência e a Tecnologia.

Abstract

Water electrolysis is a promising and environmentally friendly method to obtain hydrogen with a high degree of purity. A way to improve the efficiency of this process is through the use of catalysts. However, currently, the best electrocatalysts for this process contain rare and expensive materials belonging to the platinum group metals (PGM's). Metal phosphides, like nickel (Ni), cobalt (Co) and iron (Fe), have emerged as good candidates to catalyse the hydrogen evolution reaction (HER). The present work aims to develop earth-abundant transition metal phosphides (TMP's) to be used as catalysts in water electrolysis, in order to reduce its operating costs in comparison with the actual use of platinum (Pt).

In this sense, binary M-P (M = Ni, Co, Fe; P = Phosphide) nanoparticles (NP's) supported on carbon black (CB) were synthesised by incipient impregnation method. In order to increase the conductivity and surface area of the support, the carbon material was previously functionalized by introducing oxygenated and nitrogen groups at its surface, by oxidation with nitric acid and by N-doping using melamine as nitrogen precursor. Subsequently, the developed catalysts were characterized by N_2 adsorption-desorption equilibrium isotherms at -196 ºC, Transmission Electron Microscopy (TEM), X-Ray Diffraction (XRD), Thermogravimetric Analysis (TG), Temperature Programmed Desorption (TPD), Elemental Analysis (EA) and Linear Sweep Voltammetry (LSV) to finally be applied in the HER.

It were used cost-effective and fully reproducible preparation procedures of the phosphide NP's, feasible for large-scale production. It was demonstrated that both phosphorization and carbon functionalization have a positive influence in the electrochemical results in terms of activity and stability. Key kinetic parameters such as Tafel slope was determined for the most promising catalysts, being obtained Tafel slopes of 77 and 122 mV dec^{-1} for CoP 20%/CB_O and CoP 20%/CB_N, respectively, larger than that reported for Pt/C, but still quite acceptable. In addition, the TMP's demonstrate to have admirable stability during prolonged operation, thus, with some improvements to be developed, TMP's can be an emerging class of materials capable of replacing PGM's in water electrolysis.

Keywords: Water electrolysis, TMP's, PGM's, HER

Resumo

A eletrólise da água é uma tecnologia promissora e amiga do ambiente para produzir hidrogénio com um elevado grau de pureza. Uma forma de melhorar a eficiência deste processo é através do uso de catalisadores. No entanto, atualmente, os melhores eletrocatalisadores para este processo contêm metais raros e caros pertencentes aos metais do grupo da platina (MGP). Os fosfetos de metais, tais como o níquel (Ni), cobalto (Co) e ferro (Fe), têm vindo a ser considerados bons candidatos para catalisar a reação de evolução do hidrogénio (REH). O presente trabalho tem como objetivo o desenvolvimento de fosfetos de metais de transição (FMT) abundantes, para serem usados como catalisadores na eletrólise da água, de forma a reduzir os seus custos de operação em comparação com o uso atual da platina (Pt).

Neste sentido, foram sintetizadas, pelo método de impregnação incipiente, nanopartículas de fosfetos de metais de transição suportadas em negro de carbono. Com o objetivo de aumentar a condutividade e a área superficial do suporte, o material de carbono foi funcionalizado através da introdução de grupos oxigenados e azotados na sua superfície, respetivamente, por oxidação com ácido nítrico e por dopagem com azoto usando melamina como precursor. Posteriormente, os catalisadores desenvolvidos foram caraterizados por isotérmicas de equilíbrio de adsorção-dessorção de azoto a -196 ºC, Microscopia Eletrónica de Transmissão (MET), Difração de Raios-X (DRX), Análise Termogravimétrica (TG), Dessorção a Temperatura Programada (DTP), Análise Elementar (AE) e Voltametria Linear (VL), para finalmente serem aplicados na REH.

Foram utilizados procedimentos de preparação eficazes a nível de custo e totalmente reprodutíveis das nanopartículas de fosfetos de metais de transição, viáveis para produção em grande escala. Foi demostrado que tanto a fosforização como a funcionalização do material de carbono têm uma influência positiva nos resultados eletroquímicos em termos de atividade e estabilidade. Parâmetros cinéticos importantes como o declive de Tafel foram determinados para os catalisadores mais promissores, tendo sido obtidos declives de Tafel de 77 e 122 mV dec^{-1} para as amostras CoP 20%/CB_O e CoP 20%/CB_N, respetivamente, que são mais elevados que o valor reportado para a Pt/C, mas ainda assim bastante aceitáveis. Além disso, os FMT demostraram uma estabilidade notável durante operação prolongada, pelo que, com algumas melhorias a serem implementadas, os FMT poderão ser uma classe emergente de materiais capazes de substituir os MGP na eletrólise da água.

Palavras-chave: Eletrólise da água, FMT, MGP, REH

Declaration

I hereby declare, on my word of honor, that this work is original and that all non-original contributions were properly referenced with source identification.

Diogo Miguel Marques Abreu

October of 2018

Index

List of Figures

List of Tables

Notation and Glossary

BET	Brunauer-Emmett-Teller	
BJH	Barrett-Joyner-Halenda	
b	Tafel Slope	mV dec^{-1}
CB	Carbon Black	
CNS's	Carbon Nanospheres	
CNT's	Carbon Nanotubes	
Co	Cobalt	
CP	Carbon Paper	
DFT	Density Functional Theory	
dp	Diameter of the Particles	nm
EA	Elemental Analysis	
Fe	Iron	
HER	Hydrogen Evolution Reaction	
i	Electric Current	A
j	Current Density	mA cm^{-2}
j_0	Exchange Current Density	mA cm^{-2}
LSV	Linear Sweep Voltammetry	
m	Mass	g
MEA	Membrane Electrode Assembly	
Ni	Nickel	
NP's	Nanoparticles	
NS's	Nanosheets	
OER	Oxygen Evolution Reaction	
PEM	Polymer Electrolyte Membrane	
PGM's	Platinum Group Metals	
Pt	Platinum	
RHE	Reversible Hydrogen Electrode	
SCE	Standard Calomel Electrode	
S_{BET}	Surface area calculated by the BET method	$m^2\ g^{-1}$
S_{meso}	Mesopore surface area	$m^2\ g^{-1}$
TEM	Transmission Electron Microscopy	
TG	Thermogravimetric Analysis	
TMP's	Transition Metal Phosphides	
TPD	Temperature Programmed Desorption	
TPR	Temperature Programmed Reduction	
V_{micro}	Micropore Volume	$cm^3\ g^{-1}$
V_p	Pore Volume	$cm^3\ g^{-1}$
XRD	X-Ray Diffraction	
η	Overpotential	mV
η_{onset}	Onset Potential	mV

Greek Letters

θ	Angle	°
λ	Wavelength	Å

1 Introduction

1.1 Framing and presentation of the work

Catalysis is a research field that affects and changes our lives much more profoundly than we realize. Without the synthesis of ammonia through heterogeneous catalysis, mankind would be confronted with a serious shortage of food. On the other hand, homogeneous catalysis is the basis of the biological energy conversion of sunlight and thus responsible for all the energy that we consume in addition to food. In addition, technical energy conversions in combustion and in batteries are governed by heterogeneous electrocatalytic processes. The complexity of a catalyst function, together with its inherent material dynamics, render the field of catalysis a major challenge.

Hydrogen has being considered a renewable energy with strong potential to substitute the fossil fuels that currently are in the base of the world economy. Water electrolysis is the most important method to obtain hydrogen with a high degree of purity. It is a promising and environmentally friendly technology that involves the decomposition of water into oxygen and hydrogen gas due to an electric current passed through the water. However, there are some improvements to be achieved before hydrogen production through water electrolysis becomes competitive in relation to other available technologies. In fact, currently, the best electrocatalysts for this process contains rare and expensive metals belonging to the platinum group (PGM's), which limits its application in real conditions. In this context, this dissertation arises from the need to develop robust electrocatalysts composed exclusively of abundant and cheap materials, presenting high activity and stability similar to the PGM's.

The main goal of this dissertation is to explore the electrocatalytic properties of transition metal phosphides (TMP's) like phosphide nanoparticles (NP's) of nickel (Ni), cobalt (Co) and iron (Fe) supported in carbon black (CB). The electrocatalysts developed were characterized by a set of techniques such as N_2 adsorption-desorption isotherms at -196 ºC, Transmission Electron Microscopy (TEM), X-Ray Diffraction (XRD), Thermogravimetric Analysis (TG), Temperature Programmed Desorption (TPD), Elemental Analysis (EA) and Cyclic Voltammetry (CV). Finally, the synthesized electrocatalysts were tested in the HER.

The electrocatalysts were prepared, characterized and tested in the International Iberian Nanotechnology Laboratory (INL), in Braga, and in the Laboratory of Separation and Reaction Engineering - Laboratory of Catalysis and Materials (LSRE-LCM) located in the Faculty of Engineering of the University of Porto (FEUP).

1.2 Presentation of the company: INL

The International Iberian Nanotechnology Laboratory is a research organization located in Braga. It was founded in 2005 by the Governments of Portugal and Spain, under an international legal framework, to perform interdisciplinary cutting edge research, to implement and articulate nanotechnology for the benefit of society.

At INL, scientists and engineers from all over the world dedicate themselves to scientific research of excellence in nanotechnology. Their research programme covers four fields of application of nanoscience and nanotechnology: Health, Food and Environment monitoring, Information and Communication Technologies (ICT) and Renewable Energy.

1.3 Contributions of the Work

The electrocatalysts used in the HER were prepared in the INL. In an initial phase, I synthesized TMP nanocatalysts supported on carbon black functionalized with different groups, by following well-defined preparation procedures with help from my advisor, Dra. Juliana Sousa, in the phosphorization step. Later, I tested the prepared electrocatalysts on HER and evaluated their stability. I also compared the performance of the materials with the activity of commercial Pt/C. Still at INL, some functional characterization techniques such as TEM and XRD were conducted by Dra. Juliana Sousa.

In FEUP, I finalized the preparation of the catalysts and further explored the potential and stability of the as-prepared catalysts by carrying out N_2 isotherms, TG, TPD, EA and Chronopotentiometry, using for this purpose the equipments located in the LSRE-LCM facilities.

1.4 Organization of the thesis

The present dissertation is divided in six chapters. The first Chapter introduces the subject of the work, contextualizing the objectives. Regarding Chapter 2, it corresponds to the “Context and State of the Art”, where several types of catalysts that already exist for the desired application are presented and its respective results. In Chapter 3, titled “Materials and Methods”, it is described the design of the several catalysts and the methods used for their characterization. It is also explained how the electrochemical tests were performed in order to evaluate their activities for HER. In Chapter 4, called “Results and Discussion”, all the results are presented and discussed. In Chapter 5, “Conclusions”, the general conclusions of the work are presented. Finally, in Chapter 6, “Assessment of the Work done”, it is mentioned whether the initial objectives were achieved as well as limitations and future work, suggesting other approaches which may complement the work carried out in this project.

2 Context and State of the Art

Industrialization has been providing changes in human activity over the past years, originating an automated society, in which electricity is the base of all functioning. Currently, the society lives in a time of change, not always aware of the factors responsible for the environmental impacts and whose predictions for the future only tend to increase. In fact, the society is very dependent of fossil fuels for energy production and this leads to serious consequences, such as the increase of environmental pollution and fast depletion of natural resources [1]. In recent years it has been observed an increasing demand for alternative energy sources. The obligation to implement new energy frames can lead to a decreased dependence on hydrocarbons, responding in an appropriate way to the growth of emerging economies, involving the use of renewable energy as a primary source of energy [2].

In this sense, hydrogen is considered an important energy carrier and storage media for a future "Hydrogen Economy". Hydrogen offers a future sustainable energy for both transport and stationary applications with near zero greenhouse gas emissions, especially when generated through electrolysis of water [3].

Electrolysis is considered a clean and renewable method to produce hydrogen from water. It is a mature technology based on the generation of hydrogen and oxygen by applying a direct electric current to water to dissociate it. Hydrogen obtained with this technology has a high purity that can reach 99.999 vol. % [4]. In the electrocatalytic water splitting process, oxygen gas is generated at the anode due to the Oxygen Evolution Reaction (OER), a slow electrochemical reaction as compared with the Hydrogen Evolution Reaction (HER), whereas hydrogen is generated at the cathode [5].

Electrolysis can be distinguished according to the type of electrolyte used. The two main water electrolysis technologies to produce hydrogen are alkaline electrolysis [6] and proton exchange membrane (PEM) electrolysis [7]. In conventional PEM water electrolyzers, platinum (Pt) is used as electrocatalyst for the HER and iridium oxide (IrO_2) is used for the OER [8].

An acidic membrane, usually Nafion, is used as solid electrolyte instead of a liquid electrolyte. The membrane conducts H^+ ions from the anode to the cathode and separates hydrogen and oxygen that are produced in the reaction. The anode, cathode, and membrane set constitute the so-called Membrane Electrode Assembly (MEA). The kinetics of the hydrogen and oxygen production reactions in PEM electrolysis are faster than in alkaline electrolysis due to the acidic nature of the electrolyte and due to the metal surface of the electrodes [9]. The main advantages of PEM electrolyzers are that it can operate at much higher current densities and can work under a wide range of power input [10].

However, so far water electrolyzers have not been widely deployed, mainly because the hydrogen produced from water electrolysis is still not economically competitive [11]. Presently, the electrocatalysts that present the best performance in water electrolysis are made with metals that belong to PGM's. However, in addition to be expensive, PGM's also have limited availability in the earth's crust, not being practical to implement electrolyzers containing these rare metals on a large scale [12]. So, to reduce the production cost of the electrocatalysts, low-cost and earth-abundant electrocatalysts for HER and OER based on transition metals, such as Ni, Co and Fe are being developed [13].

Transition metal phosphides (TMP's) have been developed in recent years, showing excellent HER electrocatalytic performance [14]. So, how to enhance the electrocatalytic activity of these metal phosphides based catalysts has been the main focus of many researchers.

On the other hand, it is well known that the electrical conductivity and surface area are important factors that directly influences the efficiency of the electrocatalysts. Carbon materials are ideal supports to enhance the electrocatalytic activity due to their unique set of properties, such as physical stability, high electrical conductivity and large surface area [15]. In addition, it is possible to functionalize the carbon surface, creating different types of oxygen, sulphur or nitrogen groups on the surface that modify the physical and chemical properties of the carbon, therefore obtaining more active sites [16]. Furthermore, this process can produce carbon-based materials with improved ability to adsorb the atomic/molecular species undergoing catalytic reactions and without substantially compromise their conductive properties [17]. These heteroatoms doped structures may provide opportunities for further developing low-cost PGM-free catalysts with higher activities and longer lifetimes.

Among carbon materials, carbon black (CB) is probably the most accessible and cost-effective, and has been widely used in both research and industry [18]. It offers a great versatility due to its porous texture that can be easily tailored, yielding high surface area supports, and also due to its chemical inertness, which avoids harmful metal–support interactions. Indeed, CB is found as a support for a wide range of catalysts such as noble metals and earth-abundant materials.

2.1 Water Electrolysis

The implementation of the so-called "Hydrogen Economy" has been disrupted by the fact that, even though hydrogen is the most abundant element in the universe, it cannot be found in its pure state in the nature. In fact, the main processes to produce hydrogen are from fossil fuels, including steam reforming and partial oxidation of hydrocarbons. Renewable hydrogen can also be obtained from biomass through the same thermochemical processes [4].

Nevertheless, steam reforming of fossil fuels produces low purity hydrogen with a high concentration of carbonaceous species such as carbon monoxide. More importantly, steam reforming does not relieve dependencies on scarce fossil fuels or reduce their pollutants, therefore not contributing to the establishment of a "Carbon-Balanced" energy matrix [10].

In this context, hydrogen production methods based on fossil fuels are considered transitional technologies. On the other hand, water is an abundant and renewable resource of great importance and it is widely agreed to be the most interesting source of sustainable hydrogen in the future [4,10].

2.1.1 Principle

Water electrolysis consists in circulating a direct current through water to separate its molecules into hydrogen and oxygen. The current flows between two electrodes separated and immersed in an electrolyte to raise the ionic conductivity. The electrodes have to be resistant to corrosion, have a good electric conductivity, exhibit good catalytic properties and show a suitable structural integrity. The electrolyte has to be prevented from having any change during the process, therefore it is important for it not to react with the electrodes [4].

During the electrolysis process it is important to implement a diaphragm in order to avoid the recombination of the hydrogen and the oxygen generated. Nevertheless, the diaphragm should have a high ionic conductivity and has to show both physical and chemical high stability [4,10]. The electrodes, the diaphragm, and the electrolyte are the elements that configure the electrolytic cell. Equation 1 reveals the global electrolysis reaction.

$$H_2O\ (l) \rightarrow H_2\ (g) + \tfrac{1}{2}\ O_2\ (g) \qquad (1)$$

In addition, the operating principle of a water electrolysis cell is illustrated in Figure 1.

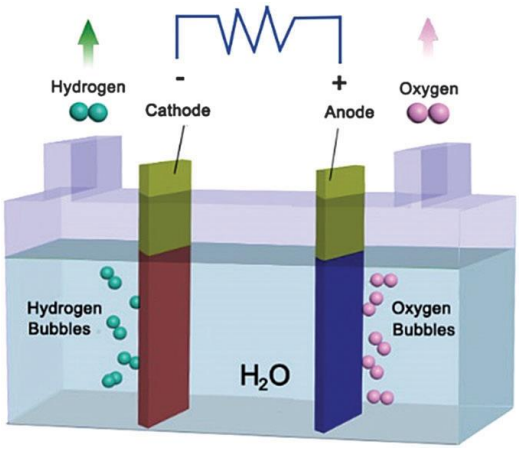

Figure 1 - Schematic diagram of an electrolyzer [19]

In the electrolysis process, the electrons are taken or released by the ions at the electrodes surface, generating a multiphasic gas–liquid–solid system. Thus, the water splitting reaction can be divided into two half-reactions: the HER which takes place at the cathode, where electrons flow from the outside circuit to this electrode and polarize it negatively; and the OER that occurs at the anode. The electrons leave the anode to the outside circuit, polarizing it positively. Hydrogen is hence generated at the cathode and oxygen at the anode [4,19].

2.1.2 Hydrogen Evolution Reaction (HER)

In an acidic media, HER normally occurs on the catalyst surface in one of two different step methods and can follow either the Volmer–Heyrovsky mechanism or the Volmer–Tafel mechanism [20]. These are represented in the Equation 2, 3 and 4.

Volmer Step:

$$H_3O^+ + e^- \rightarrow H_{ads} + H_2O \quad (2)$$

Heyrovsky Step:

$$H_{ads} + H_3O^+ + e^- \rightarrow H_2 + H_2O \quad (3)$$

Tafel Step:

$$H_{ads} + H_{ads} \rightarrow H_2 \quad (4)$$

If the catalyst surface does not present enough H adsorption sites and its surface is partially covered with adsorbed H atoms (H_{ads}), it will undergo electrochemical desorption and follow the Volmer–Heyrovsky mechanism (Equation 2 and 3). At a low overpotential, the Heyrovsky step will be the rate-determining step. On the other hand, if the catalyst surface has a high coverage of H_{ads}, it may follow the Volmer–Tafel mechanism (Equation 2 and 4) and the Tafel step will then be the rate-determining step at a low overpotential [20,21].

2.1.3 Oxygen Evolution Reaction (OER)

In OER, molecular oxygen is produced via several proton/electron coupled procedures. This reaction is highly pH dependent and, in acidic conditions, two water molecules (H_2O) are oxidized into four protons (H^+) and oxygen molecule (O_2) [22]. OER is reflected in Equation 5 for acidic media.

$$2\ H_2O \leftrightarrow 4H^+ + O_2 + 4e^- \quad (5)$$

Compared to the HER, the OER is more difficult to accomplish as it is a thermodynamically and kinetically demanding process involving four sequential proton-coupled electron transfer steps and the O=O bonding formation, resulting in slow kinetics and large overpotentials [22,23].

2.1.4 Electrocatalysts for HER and OER

There are few catalysts that are able to catalyse both HER and OER in the same electrolyte [12]. So, developing a bifunctional catalyst that is capable of catalysing both HER and OER, two half reactions occurring in the same electrolyzer, could be very attractive, since it can simplify the fabrication procedure of electrolyzers and substantially decrease the production cost.

Up to present, a variety of transition metal compounds such as molybdenum sulfide, molybdenum boride, molybdenum nitride, molybdenum selenium, molybdenum carbide, nickel phosphide, iron phosphide, cobalt phosphide and tungsten phosphide have emerged as attractive HER electrocatalysts [15,24]. However, their catalytic performances are still low as compared to noble metal catalysts; and, in order to enhance their catalytic activities, a lot of approaches have been attempted by many researchers.

For example, Ma *et al.* [25] report a highly active electrocatalyst composed of MoS_2 nanosheets (NS's) on reduced graphene oxide (RGO) paper. Tang *et al.* [26] synthesized $MoSe_2$ NS's and $MoSe_2$/RGO hybrids and compared their catalytic properties. Zhang *et al.* [27] reported the synthesis of iron phosphide NP's on graphene sheets and demonstrated their high HER activity.

Also, other previous researches indicate that nanostructured nickel phosphide supported on carbon nanospheres (CNS's) and carbon nanotubes (CNT's) exhibit excellent electrocatalytic performances. For instance, Pan *et al.* [24] synthesized nanostructured nickel phosphides supported on CNS's (Ni_2P/CNS's) that exhibited excellent activity and stability for HER and are considered a promising candidate for substituting noble metal catalysts. The same authors also describe their recent efforts in developing CNT's decorated with Ni_2P NP's to enhance the electrocatalytic activity by using nickel acetylacetonate ($Ni_{(acac)2}$) as nickel source and trioctylphosphine (TOP) as phosphorus source in oleylamine (OAm) solution of CNT's. The Ni_2P/CNT nanohybrid exhibited excellent electrocatalytic activity in 0.5 M H_2SO_4 with a low onset overpotential (88 mV), a small Tafel slope (53 mV dec^{-1}) and good stability [28].

Wang *et al.* [12] report a convenient and scalable approach to the fabrication of self-supported 3D carbon paper (CP) electrode integrated with vertically aligned NiP NS's. This was realized by electrodeposition of Ni on the surface of carbon microfibers, followed by a simple one-step phosphorization process in phosphorus vapor. The authors demonstrate that the supported NiP/CP electrode can be directly used either as a cathode to drive HER or as an anode to expedite OER, exhibiting excellent catalytic activity and outstanding long-term durability.

Electrocatalytic performance of the NiP/CP electrode towards HER was evaluated in 0.5 M H_2SO_4. For comparison, the HER activity of a bare CP and commercially available Pt/C catalysts was also measured. In potentiostatic experiments, it is widely assumed that the potential drop across the interfacial region at the working electrode is the same as the potential applied between the reference and working electrode. However, this is not exactly true, since in reality there is some *iR* drop between the two electrodes due to solution resistance.

Figure 2a shows the *iR*-corrected polarization curves of the bare CP, Pt/C, and NiP/CP measured at a scan rate of 5 mV s^{-1}. As expected, Pt/C exhibits the highest activity for HER, while the bare CP only shows negligible catalytic current even at a high overpotential. In contrast, the NiP/CP electrode has a η_{onset} as low as −18 mV. The results demonstrate that it only needs small overpotentials of 98 (η_{10}), 116 (η_{20}), and 162 mV (η_{100}) to drive HER at current densities (j) of 10, 20, and 100 mA cm^{-2}, respectively [12]. Figure 2b presents the Tafel plots, overpotential (η) versus log (j), for Pt/C and NiP/CP electrodes. The Tafel slope of 31.6 mV dec^{-1} for Pt/C is consistent with the value reported in the literature [24]. The NiP/CP exhibits a Tafel slope of 58.8 mV dec^{-1}, larger than that of Pt/C, but superior to many HER catalysts reported. The slope approximately falls within the range of 38–116 mV dec^{-1}, suggesting that the HER taking place on the NiP/CP surface would follow a Volmer–Heyrovsky mechanism, and that the rate of the discharge step would be consistent with that of the desorption step. By extrapolating the Tafel plot to an overpotential of 0 V, the exchange current density (j_0) for HER on the NiP/CP is obtained, being 0.24 mA cm^{-2} [12].

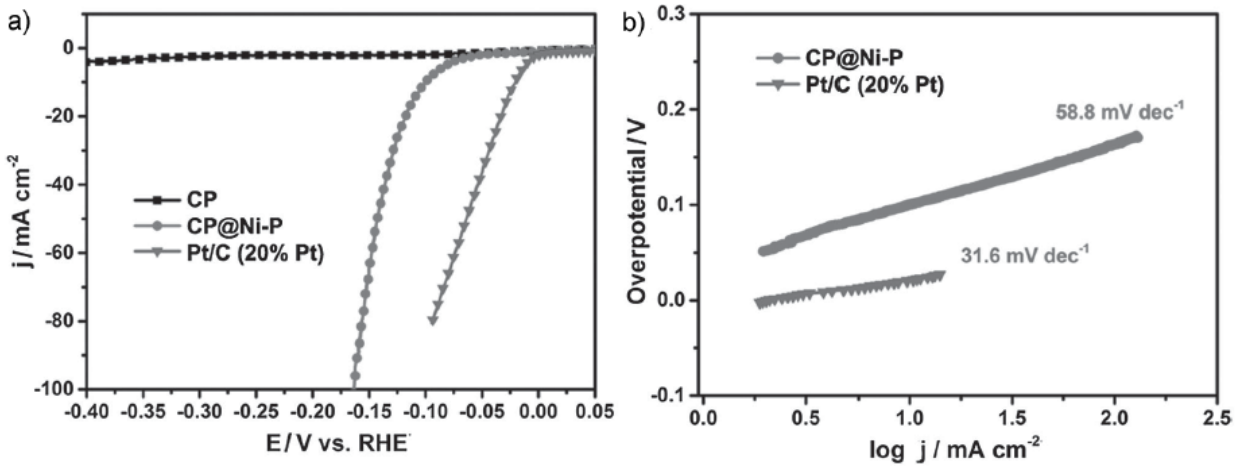

Figure 2 – a) Polarization curves of a bare CP, Pt/C, and NiP/CP recorded at a scan rate of 5 mV s^{-1}. b) Tafel plots of Pt/C and NiP/CP [12]

A durability test was performed at a fixed cathodic current density of 10 mA cm^{-2} for approximately 160 h (Figure 3), during which the overpotential was only increased from 98 to 124 mV, demonstrating excellent long-term durability of the electrode in acidic medium [12].

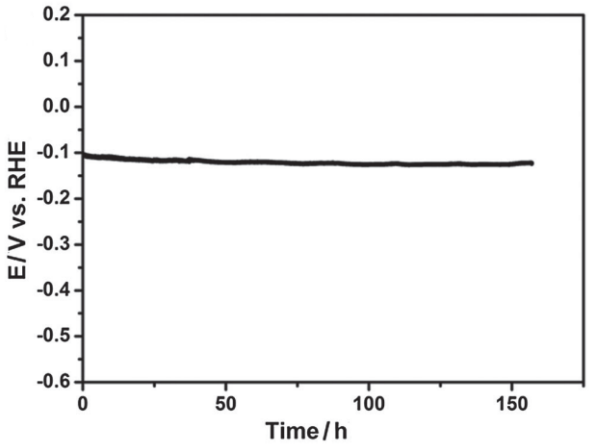

Figure 3 - Chronopotentiometric curve recorded at −10 mA cm^{-2} [12]

In this dissertation, TMP's and carbon materials such as carbon black, which is the support selected for the work, will be described in sections 2.2 and 2.3 respectively.

2.2 Transition Metal Phosphide Catalysts

As mentioned, the production of hydrogen by water splitting is an important component of several developing clean-energy technologies. HER is indeed facilitated by noble metals such as Pt. In this sense, the replacement of Pt by earth-abundant metals would be desirable in order to facilitate the global scalability of such potential clean-energy technologies.

In 2005, Rodriguez *et al.* [29] first brought forward a standpoint that Ni_2P might be the best practical catalyst for the HER according to their DFT calculation, which indicated the excellent catalytic behaviour of Ni_2P (001) towards the HER. In their study, they found that in Ni_2P the Ni concentration was diluted by the introduction of P elements. The negatively charged non-metal atoms and isolated metal atoms functioned as proton-acceptor sites and hydride-acceptor sites, respectively. In other words, the proton-acceptor sites and hydride-acceptor sites co-exist on the surface of Ni_2P (001), and this so-called "ensemble effect" would facilitate the HER. Furthermore, the relatively strong Metal−P bonds can provide transition metal phosphides with high thermal stability and hardness, as well as resistance to oxidation and chemical attack.

TMP's are an interesting class of materials and worth investigating on the nanoscale due to their wide range of properties and applications. For instance, metal-rich phosphides show excellent activity for hydrogenation reactions [30]. Inspired by the similar mechanism between HER and hydrodesulfurization where a reversible adsorption/desorption of hydrogen atoms occurs on the catalyst in both processes, metal phosphides have emerged as a novel system of HER catalysts [31].

Basically, metal phosphides have similar physical properties to ordinary metallic compounds such as carbides, nitrides, borides and silicides. They have relatively high mechanical strength, electrical conductivity and chemical stability. Different from carbides and nitrides with relatively simple crystal structures (e.g., face-centered cubic, hexagonal close-packed or simple hexagonal), the crystal structure of phosphides is based on trigonal prisms (Figure 4) due to the large radius of phosphorus atoms (~0.109 nm) that does not fit into the ordinary octahedral holes formed by closed-packed metal atoms [19,32].

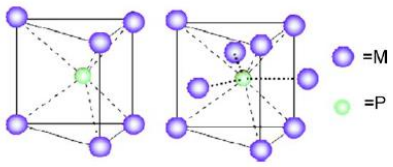

Figure 4 - Triangular prism and tetrakaidecahedral structures in phosphides [32]

Different arrangements of these blocks give rise to different structures as shown in Figure 5.

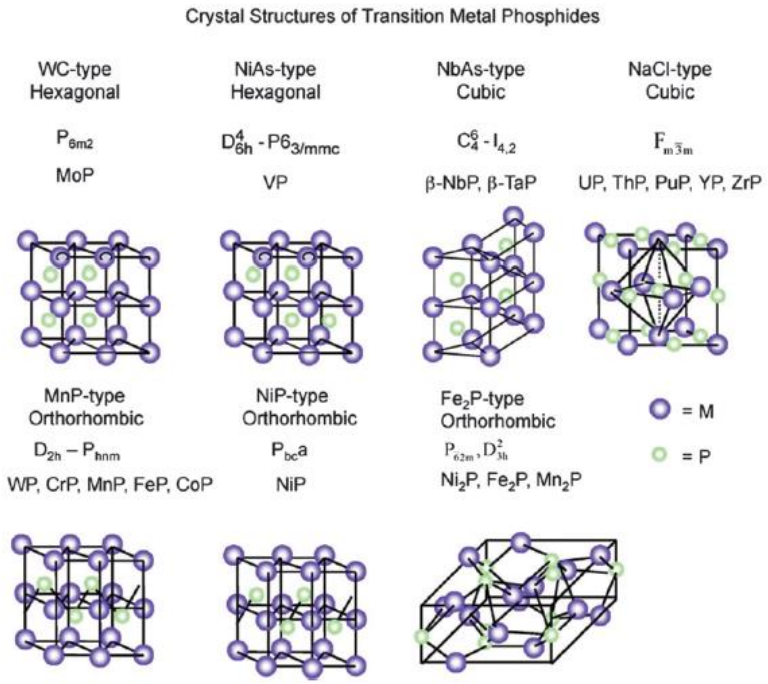

Figure 5 - Crystal structures of some transition metal phosphides [32]

These prismatic building blocks in phosphides are similar to those in sulfides. However, metal phosphides tend to form a more isotropic crystal structure, rather than a layered structure that is observed in metal sulfides [19,31,32]. This structural difference possibly results in metal phosphides having a greater number of unsaturated surface atoms than metal sulfides. Thus, metal phosphides might have an intrinsically higher catalytic activity than metal sulfides.

For catalytic applications, supported phases are often desired. Therefore, the synthesis of metal phosphides should allow the formation of nanoscale phosphides dispersed on the pore walls of a support material. This requires gas-phase or liquid-phase preparation processes so that the reagents can diffuse into the pores of the support [30].

Metal phosphides can be synthesized using a variety of methods and in various forms, including single crystals, bulk polycrystalline powders, films or nanostructured solids. Bulk metal phosphides can be prepared through traditional solid-state strategies by direct combination of the elements at high temperatures in an inert atmosphere or under vacuum [33]. Using this approach, many phosphide phases can be accessed in high purity and on a large scale. However, as is typical for bulk-scale solid-state reactions, high reaction temperatures (above 900 °C) and long reaction times (1−10 days) are generally required because these reactions depend on diffusion in the solid state [30].

In order to reduce the temperatures required by direct reactions, molten fluxes have been used in the synthesis of metal phosphides. In this approach, an unreactive and low-melting metal, such as Sn or Pb, is mixed with the precursor elements and used as a high temperature solvent to enhance the diffusion rate of the solid reagents. After the reaction, the metal matrix must be separated from the products either mechanically or by dissolution in acid [34].

Another approach that has been used in the synthesis of metal phosphides is the phosphidation of metal oxides, hydroxides, or other precursors by highly active phosphorous species. The phosphidation can be obtained either through direct exposure to phosphine gas or by exposure to related compounds generated *in situ* through the reduction of phosphate salts by hydrogen or carbon. For instance, several phosphide phases, such as Ni_2P, CoP, and FeP, can be readily obtained by temperature-programmed reduction (TPR) of the corresponding metal phosphate [32]. In a representative TPR synthesis of CoP, a stoichiometric mixture of cobalt nitrate and ammonium hydrogen phosphate is calcined in air at 500 °C for approximately 6 h to produce a cobalt phosphate precursor, which is subsequently reduced by heating to 1000 °C for 2 h in a H_2-containing atmosphere [35]. Originally developed to produce metal-oxide-supported phosphides for catalytic applications such as hydrodesulfurization or hydrodenitrogenation, the strategy has recently been extended to the production of phosphide materials directly on the surfaces of electroactive substrates, such as conductive carbon paper [36].

On the other hand, the need for high-surface-area phosphide materials for electrocatalytic applications has led to renewed interest in alternative synthetic strategies for the production of metal phosphides. For example, solvothermal reactions, thermal decomposition of organometallic precursors and reaction of organometallic compounds or metallic NP's with organophosphine reagents have been used to produce high surface area metal phosphides under reaction conditions that are milder than those of direct reactions or flux approaches.

Furthermore, these methods typically produce metal phosphides in the form of dispersible nanocrystals that can be directly applied by drop-casting or spin-coating onto the surfaces of electrodes [30,33].

In this thesis, the transition metals selected for the synthesis of the catalysts passed through Ni, Co as well as Fe, so, special attention will be given to them in the following subchapters.

2.2.1 Nickel Phosphide

In the earth's crust nickel is present at a concentration of 84 g per ton [37]. Ni-based nanocatalysis has experienced an exponential growth in the past few decades. Popczun *et al.* [38] confirmed experimentally the HER efficiency of Ni_2P NP's (~21 nm), synthesized by heating nickel (II) acetylacetonate in 1-octadecene, oleylamine and tri-n-octylphosphine (TOP). The resulting NP's were hollow and faceted to expose the (001) planes of Ni_2P. Figure 6 shows the electrocatalytic activity of these Ni_2P NP's in a typical electrochemical configuration, in 0.5 M H_2SO_4, with the working electrode prepared by deposition of the Ni_2P NP's at a mass loading of 1 mg cm^{-2} onto a 0.20 cm^2 Ti foil substrate. The as-prepared Ni_2P/Ti electrode exhibited excellent HER activity with a Tafel slope of 46 mV dec^{-1}. However, the stability of the Ni_2P/Ti electrode was not satisfactory [38].

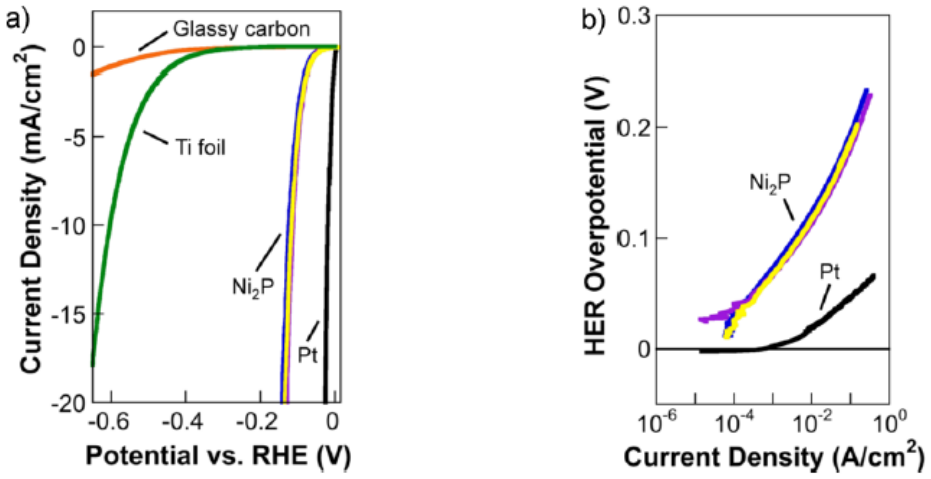

Figure 6 - a) Polarization data for three individual Ni_2P electrodes in 0.5 M H_2SO_4, along with glassy carbon, Ti foil, and Pt in 0.5 M H_2SO_4. b) Corresponding Tafel plots for the Ni_2P and Pt electrodes [38]

Kucernak *et al.* [39] investigated the effect of phosphorus content on hydrogen evolution activity and corrosion resistance in acidic medium. In their study, they used samples with different phosphorous content, including nickel–phosphorus alloy (8 at% P), $Ni_{12}P_5$ (29 at% P) and Ni_2P (33 at% P), showing that the materials with higher phosphorus content were more corrosion-resistant and more HER-active.

2.2.2 Cobalt Phosphide

Cobalt phosphide is another metal phosphide which has recently demonstrated to show great catalytic activities towards HER [40]. Sun *et al.* [41] reported their efforts in developing a nanohybrid that consists of CNT's decorated with CoP nanocrystals (CoP/CNT) by low temperature phosphidation of its Co_3O_4/CNT precursor. To examine their electrocatalytic HER activities, CoP/CNT and CoP microspheres were deposited with the same loading of 0.285 mg cm^{-2} on glassy carbon electrodes (GCE's), and the HER activities were measured in H_2SO_4 solution (0.5 M) using a typical three-electrode setup. For comparison, bare GCE, CNT, and commercial Pt/C (20 wt.%) were also examined. Figure 7a shows the polarization curves without *iR* compensation. Pt/C catalyst exhibited excellent HER activity with an overpotential close to zero. CoP/CNT exhibited a smaller onset overpotential of 40 mV and achieved current densities of 2 and 10 mA cm^{-2} at overpotentials of 70 and 122 mV, respectively, whereas CoP microspheres needed an overpotential of 226 mV to reach a current density of 10 mA cm^{-2}.

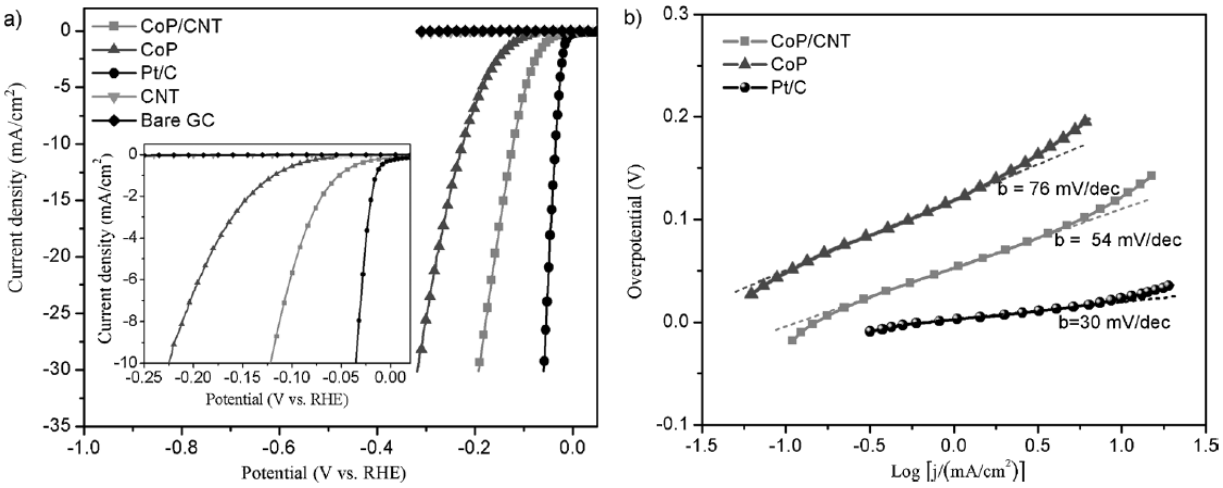

Figure 7 – a) Polarization curves for CoP/CNT, CoP, CNT, Pt/C, and bare GCE in H_2SO_4 solution (0.5 M) at a scan rate of 2 mV s^{-1}. b) Tafel plots of CoP/CNT, CoP, and commercial Pt/C [41]

The Tafel plots are shown in Figure 7b, yielding Tafel slopes of approximately 30, 76, and 54 mV dec^{-1} for Pt/C, CoP, and CoP/CNT, respectively. The measured Tafel slope for the Pt/C catalyst is close to the reported value for a commercial Pt catalyst. These Tafel slopes for both CoP catalysts reveal that the HER proceeds through a Volmer–Heyrovsky mechanism [41].

2.2.3 Iron Phosphide

Iron is the 4th most abundant element on Earth, and consequently one of the most cheap and environmentally friendly metals [37]. Callejas *et al.* [42] reported the synthesis of FeP NP's by decomposition of $Fe(CO)_5$ in a mixture of 1-octadecene and oleylamine at 190 °C and reaction

with tri-n-octylphosphine (TOP) at 340 °C for 1 h. The electrocatalytic HER activity was then evaluated in acidic (0.5 M H_2SO_4) solution. As shown in Figure 8a, when deposited on Ti foil, the FeP/Ti electrodes exhibit high HER activity with the requirement of overpotentials of -50 and -61 mV to produce current densities of -10 and -20 mA cm^{-2}, respectively.

The Tafel analysis yielded a slope of 37 mV dec^{-1} for the FeP/Ti electrodes, this slope being significantly lower than the Tafel slopes for Ni_2P (46 mV dec^{-1}) [38] and CoP (54 mV dec^{-1}) [41]. The value of exchange current density for FeP/Ti in acidic solution was 4.3 x 10^{-4} A cm^{-2}, consistent with the high activity of FeP and intermediate between that obtained for the Pt (2.49 x 10^{-3} A cm^{-2}) and Ni_2P (3.3 x 10^{-5} A cm^{-2}).

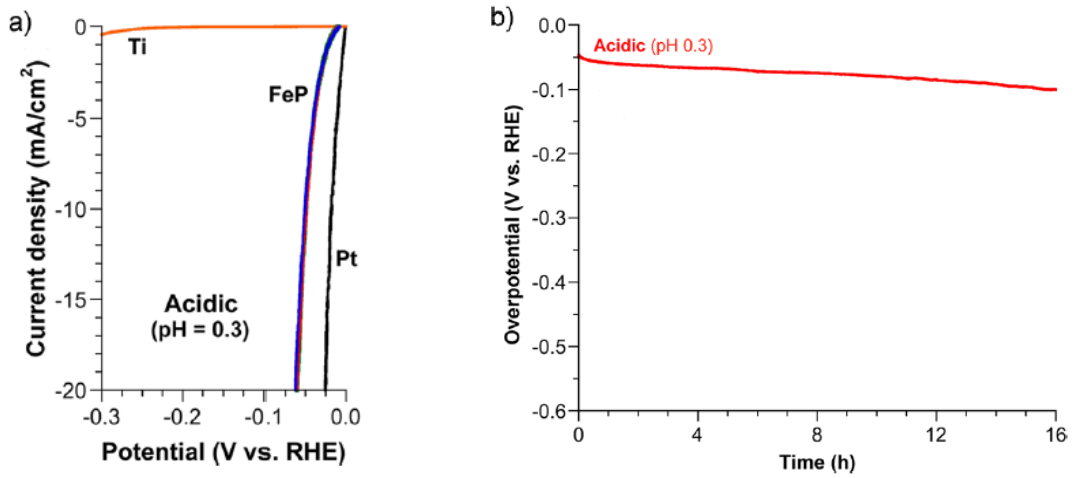

Figure 8 - a) Polarization data of FeP/Ti, Pt and Ti electrodes in 0.5 M H_2SO_4. b) Plots for FeP/Ti electrodes in 0.5 M H_2SO_4 of overpotential vs time [42]

Furthermore, the stabilities of the FeP/Ti electrodes in acidic solution were evaluated at a current density of -10 mA cm^{-2} for 16 h. Over this time period, the overpotentials increased by approximately 52 mV in acidic solution (Figure 8b), therefore exhibiting good stability [42].

2.3 Carbon Materials

Carbon materials present several properties that could be advantageous in catalysis and can offer a solution to find sustainable ways to produce chemicals, fuels and energy [43]. In fact, when applied as catalyst supports, several benefits can be found, as they are stable and inert in both acidic and basic conditions and have large surface areas. Also, carbon surfaces are relatively easy to modify by creating different functionalities that modify the catalyst acidity, polarity, and hydrophobicity. Furthermore, metal recovery from metal catalysts using a carbon support is efficient because the support can be burned off to recover the metals [18,43,44].

Carbon black, which is the support selected for this work, is widely used in catalysis applications due to its specific characteristics of stability in both acid or basic media, fineness, tunable texture and surface chemistry. Other main benefits are its high surface area and low price [45].

2.3.1 Carbon surface functionalization

The behaviour of carbon materials as support depends on their surface properties, which is determined by their structure. In general, porous carbon used in catalysis have graphitic structure. Unsaturated carbon atoms at the edges of the graphene layers and in basal plane defects can easily react with oxygen, water, or nitrogen, originating surface groups such as those represented schematically in Figure 9 [46,47]. These groups can be used to anchor catalysts or catalyst precursors, or for subsequent functionalization. In addition, they may be active sites for specific catalytic reactions. Among the oxygenated groups, carboxylic acids and anhydrides, lactones and phenols, are acidic, while carbonyl and ether groups are neutral or may form basic structures (quinone, chromene and pyrone groups). The π electrons in the basal planes also contribute to the basicity of the carbon material, affecting its adsorption and catalytic properties [48].

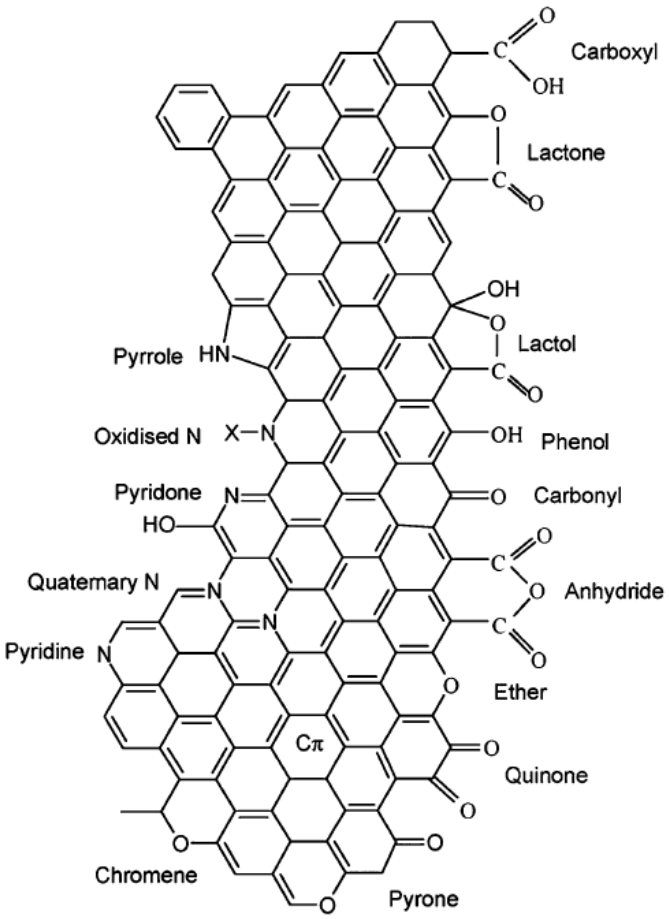

Figure 9 – Nitrogen and oxygen surface groups on carbon [46,47]

The nature and concentration of the functional groups on the surface of a carbon material can be modified by a variety of post-treatments or by changes introduced in the synthesis step. Oxygenated groups are introduced onto the carbon surface by treatment with oxidizing agents, either in the liquid phase (for example, using nitric acid) or in the gas phase (with oxygen, ozone or nitrogen oxides) [49]. This functionalization allows the formation of nanoparticles with small dimensions and uniform through a homogeneous distribution of metal precursors [50]. The oxidation extent depends on the acid concentration and on the duration of the treatment. The boiling of the carbon material in concentrated HNO_3 may lead to extensive damage into the solid with severe changes in the textural properties [49,50].

The surface oxygen-containing groups decompose by releasing CO and CO_2 (and H_2O) in different temperature ranges, as it can be seen in Figure 10.

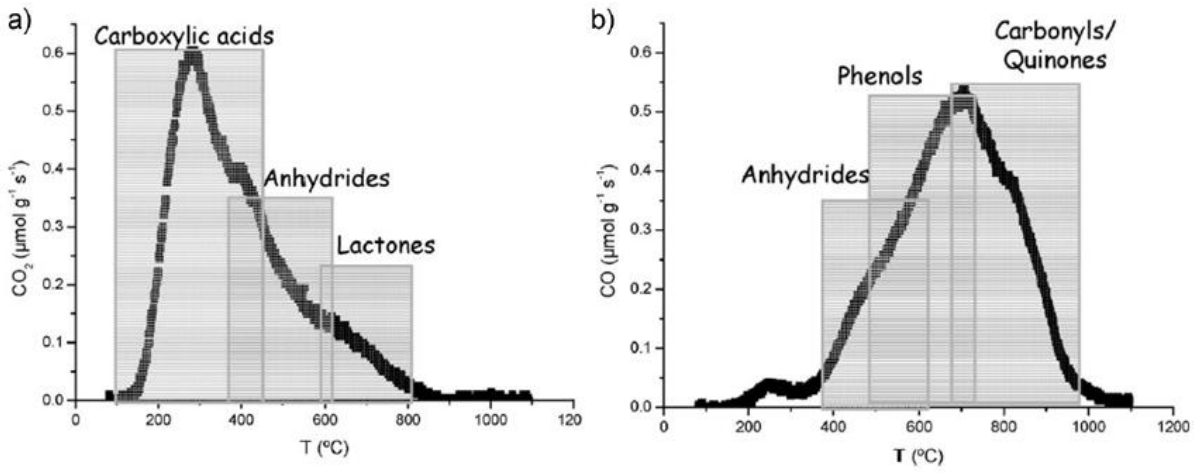

Figure 10 - Temperature ranges corresponding to the evolution of a) CO_2 and b) CO upon decomposition of the various types of oxygen functional groups [47]

Carboxylic acids release as CO_2 at low temperatures (100–450 ºC); anhydrides decompose into CO and CO_2 at intermediate temperatures (350–600 ºC); lactones release as CO_2 at higher temperatures (550–800 ºC); phenols release as CO at intermediate temperatures (500–750 ºC) and carbonyl/quinones decompose as CO at high temperatures (650–950 ºC) [46].

On the other hand, porous carbons with nitrogen functionalities can be obtained by impregnating a porous carbon with an N-containing organic compound, such as urea or melamine, followed by carbonization [46]. Nitrogen containing groups can improve the properties of the carbon for use in many applications. In fact, depending on the amount of nitrogen incorporated, the properties of carbon can be altered and often enhanced, such as the electrical conductivity, basicity, oxidation stability and catalytic activity. The performance of these materials crucially depends on the amount of nitrogen in the carbon structure [46].

Generally, the nitrogen groups incorporated include pyridine (N-6), pyrrole (N-5), oxidized nitrogen (NX) groups at the edges, and quaternary nitrogen (N-Q) incorporated into the graphene structure [46,47]. The nitrogen atoms provide additional electrons, inducing surface basicity and enhanced catalytic activity in oxidation reactions [48].

More importantly, it is also possible to exploit the control strategy used for functional groups to attach metal NP's to these carbons in a controlled way and with metal–carbon bond stabilization. This property of active sites for binding other nanoparticles can be successfully applied in metal–carbon supported catalyst systems [51], as it will be reported in this thesis by attaching Ni, Co and Fe phosphide NP's in commercial carbon black, as well as in functionalized carbon black by acidic treatment and by melamine impregnation, in order to assess their catalytic activity towards the HER.

3 Materials and Methods

The main goal of this dissertation consists in the study of the electroactivity of transition metal phosphide catalysts supported on carbon materials for the production of hydrogen.

In the following subchapters it is carried out the description of the steps, materials and equipment necessary for the synthesis of catalysts, as well as all the tests that were conducted to characterize and evaluate their efficiency in the process in question.

3.1 Synthesis of catalysts

3.1.1 Functionalization of carbon black

As mentioned previously, carbon black has attracted great attention in electrochemical applications, due to its high stability, high electrical and thermal conductivity and high specific surface area.

In order to use carbon black (CB) as a catalyst support, as it presents a high stability, it can be functionalized in order to create centres of anchorage for the metal complexes to bind. In the present work, VULCAN XC 72R carbon black was functionalized with basic and acid precursors, such as melamine and nitric acid, respectively.

3.1.1.1 Oxidation with nitric acid (HNO_3) 12 M

5 g of carbon black was put in contact with 50 mL of aqueous solution of HNO_3 12 M (65%, Sigma-Aldrich), under stirring during 6 h at room temperature. The obtained materials (CB_HNO_3) were washed with distilled water until neutral pH. Finally, it was placed in an oven at 100 °C for 24 h.

3.1.1.2 Doping with nitrogen

3 g of carbon black and 1.3 g of melamine were mixed with 100 mL of ethanol. This solution was kept in agitation for 5 h at room temperature. Then, the mixture was heated to 80 °C until all the solvent was evaporated. Finally, the carbon was placed in an oven at 100 °C for approximately 24 h. After this time, the sample (CB_N) was heat treated at 600 °C for 1 h under nitrogen atmosphere, with a heating ramp of 10 °C min^{-1}.

3.1.2 Synthesis of precursors of Ni, Co and Fe

Acetylacetonate of Ni (95%, Sigma-Aldrich), Co (97%, Sigma-Aldrich) and Fe (97%, Sigma-Aldrich) were used as source of metal. The materials were prepared with four different concentrations of metal, in particular 5, 10, 15 and 20 wt.% for each metal. For the functionalized supports, only 20% for each metal was used.

In order to find the most suitable solvent, the literature was analyzed and it was verified that the best solutions passed by dichloromethane, ethanol, acetone and isopropanol. After some tests, it was concluded that the best solvent is isopropanol for the precursors in question.

3.1.3 Impregnation of carbon materials

The different carbon materials were impregnated using the traditional incipient wet impregnation method. In a first phase, the metal precursors were dissolved in 1 mL of isopropanol solution. For each impregnation was used 1 g of carbon black with a diameter less than 180 μm. The carbon material was initially placed on ultrasound (to improve the dispersion of the metal) and the solution of the precursor was added dropwise to the carbon black. Then, the samples were placed on the ultrasound for more 90 min and then placed in a drying oven at a temperature of 110 °C for 12 h.

3.1.4 Metal reduction

After the wet incipient impregnations it was necessary to perform a hydrogen treatment to reduce the metals impregnated on the carbon materials. Temperature programmed reduction experiments were performed to determine the reduction temperature of the different metals. It was observed that to reduce nickel and cobalt it is necessary to use 500 ºC while for iron 450 ºC is enough. The treatment consisted in heating the materials in a nitrogen atmosphere with a flow rate of 100 cm^3 during 1 h with a heating ramp of 5 °C min^{-1}, and the gas was then switched to hydrogen with a flow rate of 50 cm^3 during 3 h. The materials were then cooled in nitrogen atmosphere to room temperature.

3.1.5 Phosphorization

Phosphorization of the prepared samples was carried out by gas transport. Only the samples with 20 wt.% of each metal supported on the different carbon blacks were phosphorized. For that, 0.3 g of red phosphorus (99.99%, Sigma-Aldrich) were introduced into a combustion boat and placed at the beginning of the hot zone of a tube furnace, while 0.25 g of sample was also placed in the furnace at a distance of about 3 cm of red phosphorus.

The phosphorization was conducted under continuous N_2 gas flow of 100 cm^3 min^{-1}. The system was heated to 500 °C at 10 °C min^{-1}, maintained at this temperature for 1 h and then cooled to 250 °C with a rate of 5 °C min^{-1} and held for 12 h. The as-phosphorized samples (NiP, CoP and FeP) were finally cooled and stored under ambient conditions.

3.2 Catalyst Characterization

3.2.1 N_2 adsorption-desorption equilibrium isotherms at -196 ºC

In order to characterize the textural properties of the prepared materials, it was used N_2 adsorption-desorption isotherms at -196 ºC, using the NOVA 4200e equipment from Quantachrome Instruments.

Previously to the analysis, approximately 100 mg of carbon materials were degassed, raising the temperature in a controlled way: first, the temperature was raised to 40 °C, remaining in these conditions for 2 min. Subsequently it was raised 20 °C at a time, keeping that temperature constant for 30 min, up to 350 °C. Finally, the samples were kept during 3 h at 350 °C. On the other hand, the reduced samples with metals were degassed at a temperature of 150 °C for 4 h.

The specific surface area of the as-synthesized catalysts was determined by the BET method, S_{BET}, while the external surface area, S_{meso}, and micropore volume, V_{micro} was determined by the t-method. The BJH pore size distribution method was used to calculate the pore diameter, dp, of the material's pores.

3.2.2 Transmission Electron Microscopy (TEM)

The dispersion of metals on the catalysts was described by TEM images. The tests were conducted on a probe-corrected transmission electron microscope operating at 200 kV (JEOL 2100), in the INL.

3.2.3 X-Ray Diffraction (XRD)

To analyse the phase composition of the catalysts, XRD patterns were performed in the INL. Powder XRD experiments were conducted on a X'Pert PRO diffractometer (PANalytical) set at 45 kV and 40 mA, using Cu Kα radiation (λ = 1.541874 Å) and a PIXcel detector. Data were collected using Bragg-Brentano configuration in the 2θ range of 20 ° to 80 ° with a scan speed of 0.01 ° s^{-1}.

3.2.4 Thermogravimetric analysis (TG)

The thermal behaviour of the different samples were evaluated using two different thermogravimetric procedures. First, immediate analysis was used to calculate the volatile content of the carbon materials, in order to verify if the functionalizations were well performed. For this, the equipment 409 PC LUXX of NETZSCH, located in the LCM facilities was used. The samples were heated from room temperature until 900 ºC with a heating rate of 10 ºC min^{-1} under N_2 atmosphere. This temperature was kept during 7 min under N_2 atmosphere and, after this time, the atmosphere was changed for air during 13 min.

In order to determine the metal content introduced in the different carbon materials, the following programme was performed: The materials were heated from 30 °C to 900 °C with a ramp of 5 ºC min^{-1} in air atmosphere (50 cm^3 min^{-1}).

3.2.5 Temperature Programmed Desorption (TPD)

TPD is a useful technique used for characterization of the chemical surface of the carbon materials by detection and quantification of the amounts of carbon dioxide and carbon monoxide resulting from the decomposition of oxygenated surface groups during the heating of samples. Thus, 0.1 g of the sample was placed in a U-shaped quartz tube located inside an electric furnace and heated up to 1100 °C at a rate of 5 °C min^{-1} using a constant flow of helium of 25 cm^3 min^{-1}. It should be noted that the CO and CO_2 released during the thermal analysis were monitored and calibrated at the end of each analysis. The tests were performed on the equipment AMI-300 from Altamira Instruments, equipped with AMETEK Dymaxion mass spectrometer.

3.2.6 Elemental Analysis (EA)

In order to determine the chemical composition of the carbon materials, elemental analysis was carried out on a MICRO cube analyzer from Elemental GmbH in CHNS mode. Each element (Carbon, Hydrogen, Nitrogen and Sulphur) was determined by combustion of the sample at a temperature of 1050 °C and calculated by the mean of three independent measurements, using a per-day calibration with a standard compound. On the other hand, oxygen content was carried out on a rapid OXY cube analyzer from Elemental GmbH. The composition was determined by pyrolysis of the sample at 1450 °C and calculated by the mean of three independent measurements, using a per-day calibration with a standard compound as well.

3.3 Electrocatalytic Testing

3.3.1 Preparation of the electrocatalysts

The immobilization of the transition metal phosphide nanoparticles supported on the different CB was achieved by immobilization at the working electrode using ink approach. Carbon paper was treated in a mixed solution of water, sulfuric acid and nitric acid (1:1:1) in order to introduce surface defects and oxygen groups on the carbon microfibers as essential sites for the conformal growth of metal deposits.

2.5 mg of pre-phosphorized catalyst were dispersed in a mixture of 1000 µL of ethanol and 50 µL of *Nafion* with the aid of ultrasound for 1 h. Then, 1000 µL of the dispersion was immobilized drop by drop on the working electrode with an area of 1 cm^2. The catalyst load in the working electrode was calculated, being 2.5 mg cm^{-2} for all tests performed.

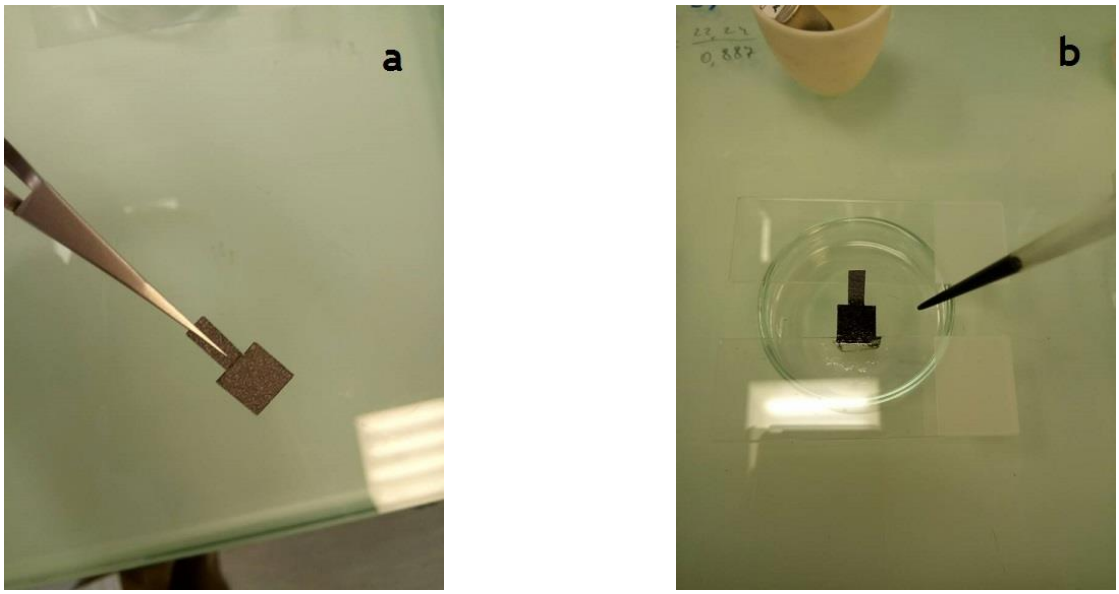

Figure 11 – Image of carbon paper before (a) and after (b) the electrocatalyst immobilization

3.3.2 Linear Sweep Voltammetry (LSV)

In order to study the electrocatalytic performance of the catalysts, LSV tests were performed in a Metrohm Autolab PGSTAT302N potentiostat/galvanostat.

To study HER, a conventional three-electrode setup was used: the working electrode, a graphite counter electrode and a saturated Calomel electrode (SCE) as the reference electrode, all immersed in an electrolyte of H_2SO_4 0.5 M, at room temperature and under stirring at 80 rpm.

The potential of the working electrode was measured between 0 V to -0.6 V, with a scan rate of 5 mV s^{-1} for 49 cycles.

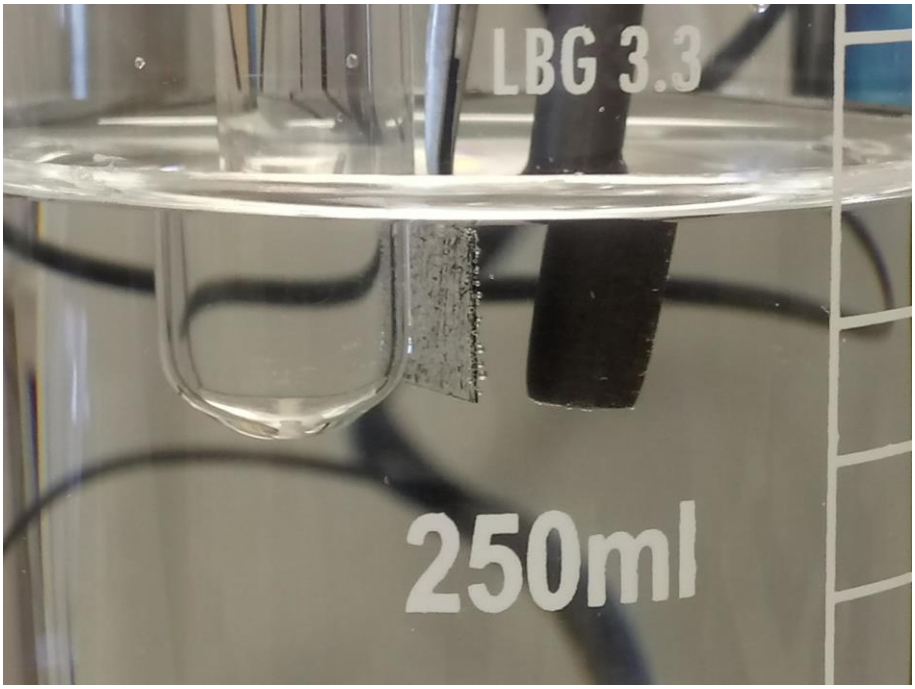

Figure 12 - Three-electrode setup used to study HER

In addition to the determination of key parameters such as Tafel slope, special attention will be given to the stability of the materials after prolonged operation in the acidic environment.

In this way, it was performed Chronopotentiometry experiments at the fixed current density of 20 mA cm^{-2} while monitoring the variation of applied potential during 12 h.

4 Results and Discussion

In this section all the results obtained in the tests described above will be discussed. In order to simplify their comparison, the catalysts were assembled into different groups, and the results of the tests performed for all carbon materials are presented in figures and tables.

4.1 N_2 adsorption-desorption equilibrium isotherms at -196 ºC

These measurements were carried out to study the textural properties (BET surface area, external surface area, pore and micropore volume, and pore size) of the as-synthesized catalysts.

The isotherms of all materials belong to type IV with a distinct hysteresis loop over a wide range of high P/P_0, which is a typical characteristic of mesoporous materials. As an example, the isotherms of the original (CB_O), oxidized (CB_HNO_3) and N-doped (CB_N) carbon blacks are shown in Figure 13.

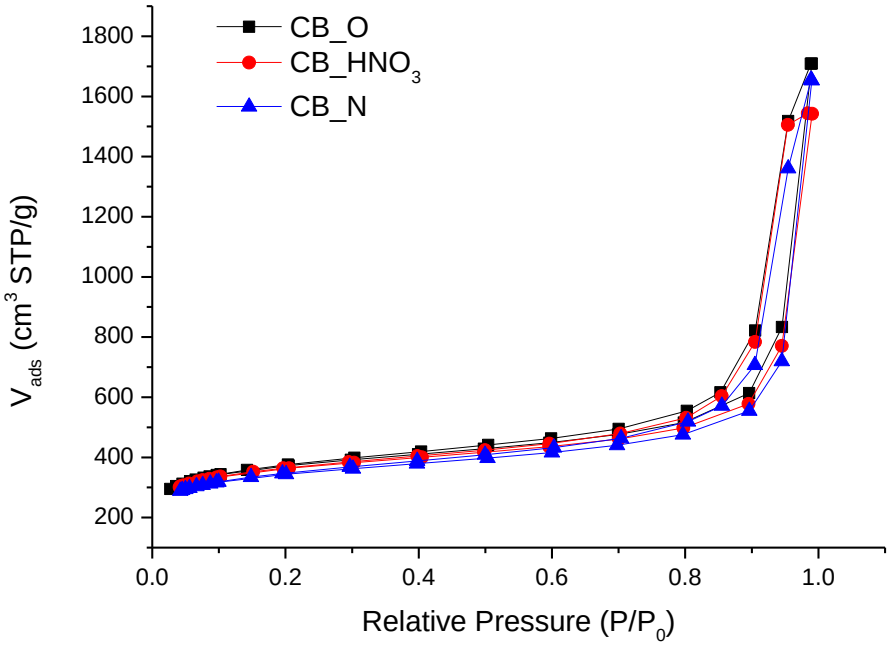

Figure 13 – N_2 adsorption-desorption isotherms of the CB samples

The textural properties values of the different carbon black samples are shown in Table 1.

Table 1 – Textural properties measured for the different supports

Sample	S_{BET} ($m^2\ g^{-1}$)	S_{meso} ($m^2\ g^{-1}$)	V_{micro} ($cm^3\ g^{-1}$)	$V_{p\ P/Po=0.95}$ ($cm^3\ g^{-1}$)	dp_{BJH} (nm)
CB_O	1265	512	0.34	1.29	32.0
CB_HNO₃	1341	491	0.33	1.19	31.8
CB_N	1266	468	0.32	1.11	32.0

Table 1 shows that the treatment with nitric acid (CB_HNO_3) slightly increases the BET surface area, while the treatment with melamine (CB_N) practically does not change the surface area of the materials. In fact, according to Soares *et al*. [52] the slight increase in the surface area of the sample oxidized with HNO_3 (CB_HNO_3) may be due to damages in the surface caused by the oxidation treatment. The same author [53] also reports that the functionalization using melamine as nitrogen precursor practically does not change the specific surface area of the support when compared to the original sample, as occurs for the CB_N sample in this work.

The mesoporous nature of the materials can be demonstrated by the higher values of mesopore surface area represented on Table 1. It was observed that after the treatments with nitrogen and oxygen groups both the mesopore area and micropore volume slightly decrease due to the introduction of these functional groups on the carbon surface. The samples CB_O, CB_HNO_3 and CB_N have a pore diameter of 32.0, 31.8 and 32.0 nm respectively. Therefore, the different treatments practically did not change the diameter of the particles.

Table 2 shows the textural properties of CB_O after metal impregnations of 5, 10, 15 and 20 wt.% and the effect of phosphorization on the CB_O materials impregnated with 20% of metal.

It was observed that the BET surface area decreases with the metal impregnation. For instance, the BET surface area of the CB_O sample decreases from 1265 $m^2\ g^{-1}$ to 1115, 1056 and to 1115 $m^2\ g^{-1}$ in cases of Ni 5%/CB_O, Co 5%/CB_O and Fe 5%/CB_O, respectively. This result was expected, since the metals were introduced inside the pores of the carbon materials, therefore decreasing the surface area of the materials. It is possible to notice that as the percentage of metal increases, both the surface area and the mesopore area decrease. In addition, generally, both pore and micropore volumes also decrease, which confirms the introduction of the metal particles into the pores of the support.

Considering the CB_O supported catalysts before and after phosphorization, it can be seen in Table 2 that this process causes a decrease of the BET surface area for the three metals. The pore volume also decreased, except for sample CoP 20%/CB_O, and the micropore volume also decreased for the three metals. This decrease can be due to the impregnated metal and due to phosphorous deposition along the surface of the support.

Table 2 – Textural properties of the catalysts supported on CB_O

Catalyst	S_{BET} ($m^2\ g^{-1}$)	S_{meso} ($m^2\ g^{-1}$)	V_{micro} ($cm^3\ g^{-1}$)	$V_{p\ P/Po=0.95}$ ($cm^3\ g^{-1}$)	dp_{BJH} (nm)
CB_O	1265	512	0.34	1.29	32.0
Ni 5%/CB_O	1115	458	0.30	1.10	32.0
Ni 10%/CB_O	1037	429	0.28	0.99	17.5
Ni 15%/CB_O	970	395	0.26	0.90	3.63
Ni 20%/CB_O	941	391	0.28	1.11	32.2
NiP 20%/CB_O	817	341	0.21	0.83	31.9
Co 5%/CB_O	1056	433	0.28	1.03	32.2
Co 10%/CB_O	1022	415	0.27	0.98	32.2
Co 15%/CB_O	905	370	0.23	0.96	32.0
Co 20%/CB_O	904	362	0.24	0.89	17.4
CoP 20%/CB_O	890	381	0.23	0.94	32.0
Fe 5%/CB_O	1115	456	0.29	1.08	31.9
Fe 10%/CB_O	1048	449	0.26	1.11	32.2
Fe 15%/CB_O	844	385	0.20	0.90	31.9
Fe 20%/CB_O	796	352	0.19	0.88	17.5
FeP 20%/CB_O	739	344	0.17	0.79	31.9

The results obtained for the catalysts with 20% of each metal supported on the functionalized carbons are shown in Table 3.

Comparing the results, it can be concluded that the impregnation of the metals cause a decrease in the BET surface area and mesopore surface area, which is more evident in the CB_HNO_3 supported catalysts. The micropore volume also decreased. It should be noticed that the thermal treatments at 500 ºC for Ni and Co and 450 ºC for Fe samples led to the release of most of the oxygen-containing groups, which are more unstable, allowing the agglomeration of the metals on the support.

Comparing the CB_HNO_3 and CB_N supported catalysts before and after phosphorization, it appears that the BET surface area decreased for the three metals after the phosphorization. For example, the BET surface area decreases to 571, 489 and to 524 $m^2\ g^{-1}$ in cases of NiP 20%/CB_HNO_3, CoP 20%/CB_HNO_3 and FeP 20%/CB_HNO_3, respectively, in relation with the values obtained for the Ni 20%/CB_HNO_3 (663 $m^2\ g^{-1}$), Co 20%/CB_HNO_3 (688 $m^2\ g^{-1}$) and Fe 20%/CB_HNO_3 (643 $m^2\ g^{-1}$) samples, further confirming that the phosphorization was well conducted. It can also be observed that both pore and micropore volume decreased, this effect being once again more noticeable in the case of the CB_HNO_3 materials for the reasons described above.

Table 3 – Textural properties of the catalysts supported on the functionalized CB

Catalyst	S_{BET} ($m^2\ g^{-1}$)	S_{meso} ($m^2\ g^{-1}$)	V_{micro} ($cm^3\ g^{-1}$)	$V_{p\ P/Po=0.95}$ ($cm^3\ g^{-1}$)	dp_{BJH} (nm)
Ni 20%/CB_HNO₃	663	312	0.16	0.74	31.9
Co 20%/CB_HNO₃	688	317	0.17	0.75	31.8
Fe 20%/CB_HNO₃	643	305	0.15	0.75	17.4
NiP 20%/CB_HNO₃	571	269	0.13	0.66	31.9
CoP 20%/CB_HNO₃	489	230	0.12	0.53	3.60
FeP 20%/CB_HNO₃	524	244	0.13	0.63	17.4
Ni 20%/CB_N	860	361	0.22	0.89	32.1
Co 20%/CB_N	714	399	0.14	0.81	3.64
Fe 20%/CB_N	769	327	0.20	0.82	17.4
NiP 20%/CB_N	740	307	0.19	0.74	17.5
CoP 20%/CB_N	457	296	0.07	0.55	3.59
FeP 20%/CB_N	651	289	0.16	0.73	17.4

4.2 TEM

TEM analysis were carried out only for selected samples taking into account the electrochemical results.

Figure 14a shows a TEM image of sample Co 20%/CB_O. It is possible to observe a large amount of Co NP's on the surface of carbon black. This result can justify the fact that the surface area of this sample is lower than the surface area of the support. The image illustrates that the Co NP's exhibit sphere-like morphology where few aggregated NP's can be observed, indicating that the Co NP's are well dispersed. Figure 14b shows the distribution of the particle size for this catalyst, indicating that the particle size is between 10 and 73 nm. However, most of the particles have a size of 17 nm.

Figure 15a illustrates the Co 20%/CB_N sample, where it can be seen that the Co NP's also exhibit a spherical shape. In spite of the particles being well dispersed, it is possible to observe the presence of some agglomerates. Particle size distribution (Figure 15b) shows that most of the metal particles presents a size between 33 and 46 nm, but particles with larger diameter, up to 182 nm were also observed. This particles with bigger size should correspond to the agglomerates.

Figure 16a shows the TEM image of the CoP 20%/CB_O sample, revealing that CoP NP's presents a spherical shape with high density and good distribution. No aggregated NP's can be observed, which indicates that the CoP NP's are well dispersed. Particle size distribution (Figure 16b) indicates that the particle size ranges between 4.0 and 12.1 nm, but most of the metal particles presents a size between 9.4 and 10.3 nm.

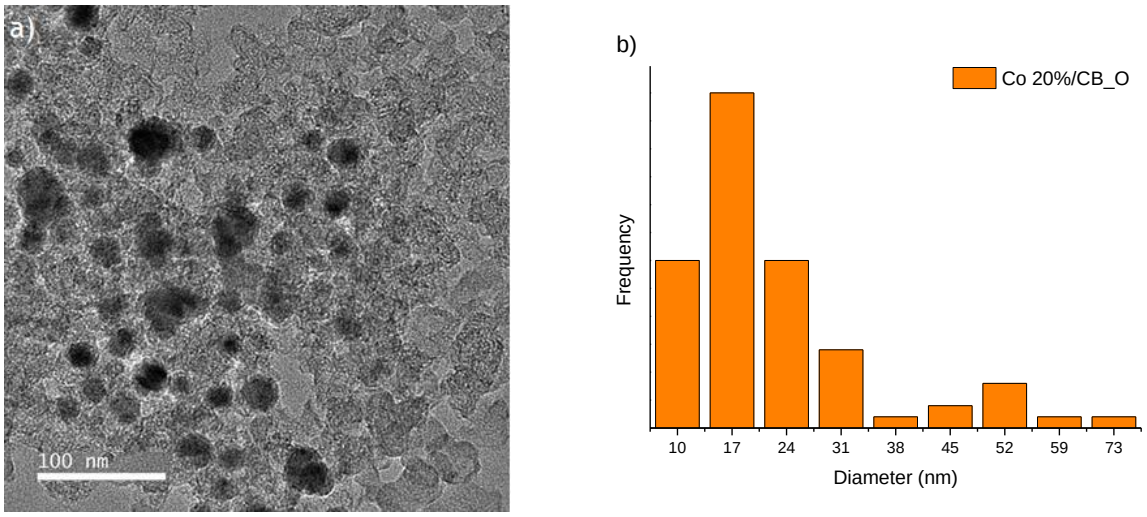

Figure 14 – a) TEM image of Co 20%/CB_O and b) respective particle size distribution

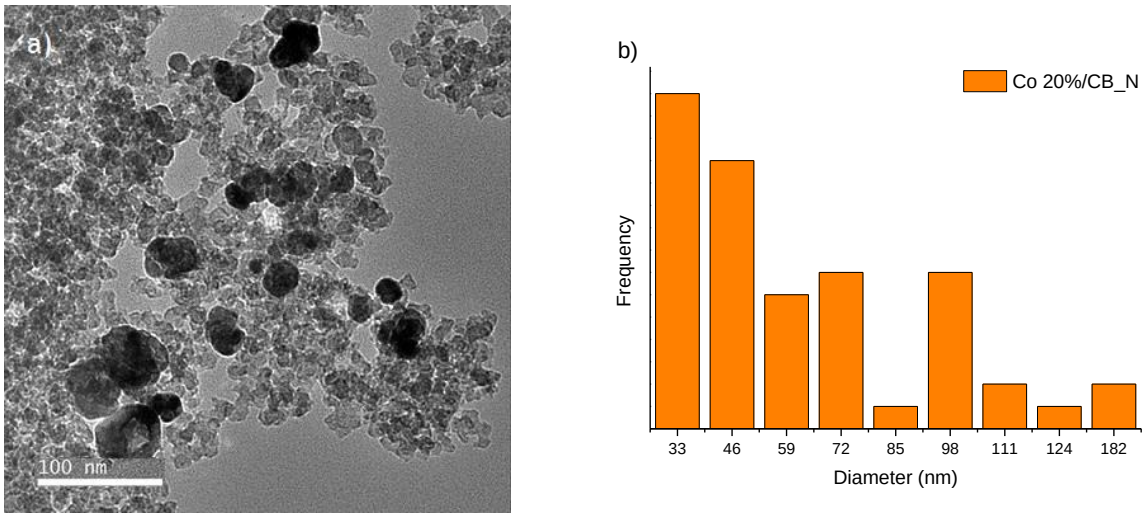

Figure 15 – a) TEM image of Co 20%/CB_N and b) respective particle size distribution

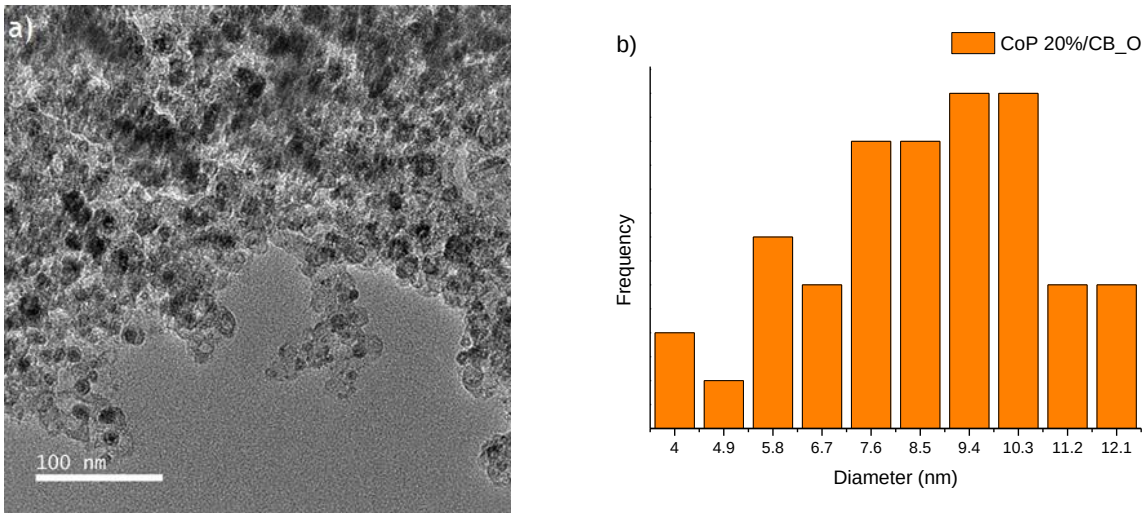

Figure 16 – a) TEM image of CoP 20%/CB_O and b) respective particle size distribution

TEM image of the sample CoP 20%/CB_N is shown in Figure 17a. These NP's show spherical morphology with good dispersion. However, just like in Co 20%/CB_N case, some nanoparticles have undergone aggregation, although less noticeable. Figure 17b shows the particle size distribution histogram, indicating that the particle size ranges between 2.0 and 18.2 nm with an average of 7.4 nm.

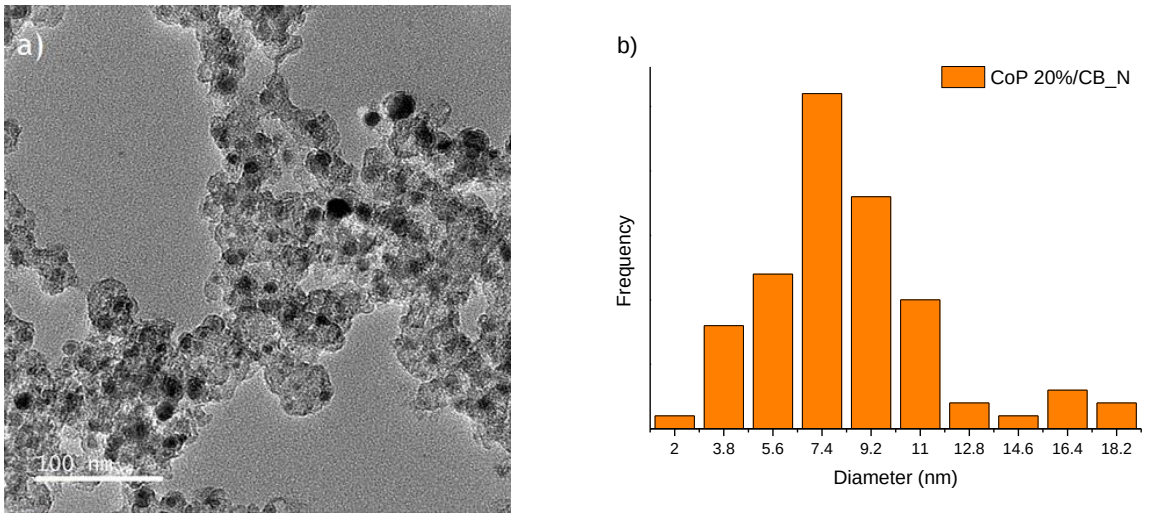

Figure 17 – a) TEM image of CoP 20%/CB_N and b) respective particle size distribution

It can be concluded that the introduction of N-groups originate particles with a broader range of diameters and can lead to the formation of agglomerates, while the deposition of phosphorous allows the formation of smaller nanoparticles and leads to a more homogeneous distribution.

4.3 XRD

The structure and composition of the materials were also analyzed by XRD, whose patterns are shown in Figures 18, 19 and 20 for Ni, Co and Fe supported catalysts, respectively.

Figure 18a illustrates diffraction peaks at 27.9 ° that can be attributed to a plane of hexagonal graphite (c), since the support is a carbon material. From the XRD spectra it is possible to conclude that the reduction process was well performed, since it was not observed the presence of nickel oxide. The XRD spectra shows the presence of cubic Ni_4 phase (COD 96-210-0662).

Observing Figure 18, it appears that the phosphorization process was well conducted, since the samples present phosphorous in their composition. In addition, it appears that the thermal treatment involved in the phosphorization promoted the appearance of different phases and crystalline compositions for the obtained phosphides. The patterns represented in Figure 18b

are consistent with that reported for nickel phosphide [38, 39]. In fact, the peaks at 40.6 °, 44.8 °, 47.4 ° and 54.3 ° can be attributed to the cubic P-rich NiP_2 phase (COD 96-901-2504) for NiP 20%/CB_O, to the hexagonal Ni_5P_4 phase (COD 96-221-4343) for NiP 20%/CB_HNO_3 and to the orthorhombic NiP_2 phase (COD 96-901-4042) for NiP 20%/CB_N.

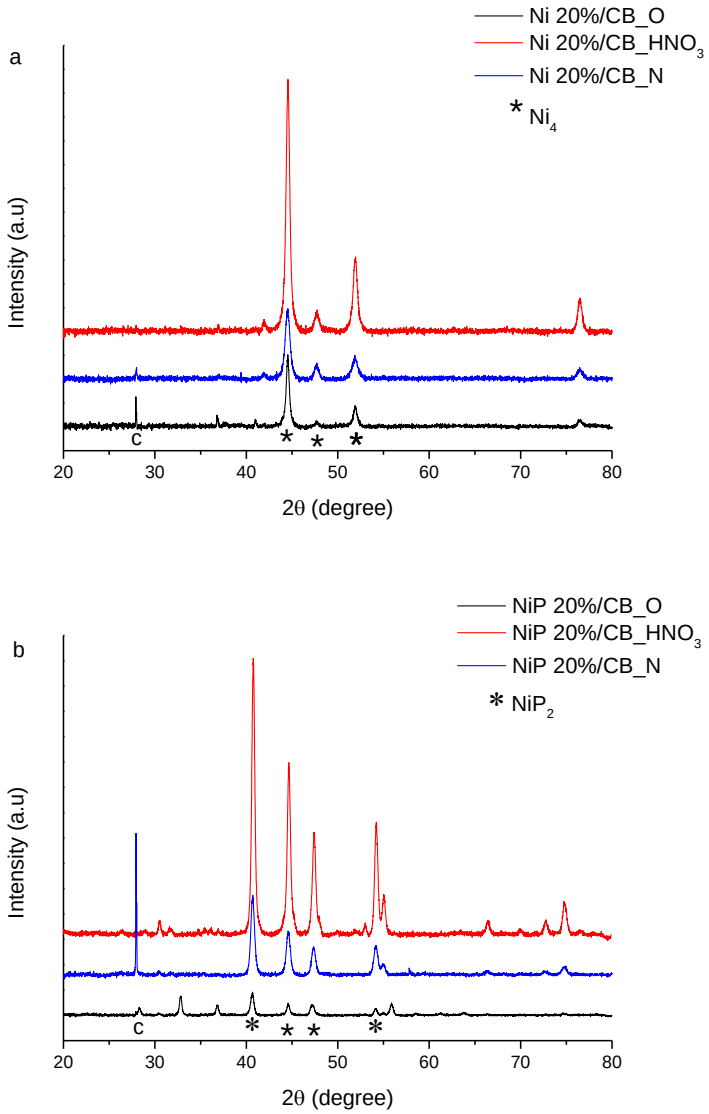

Figure 18 – XRD Patterns of Ni catalysts before (a) and after (b) phosphorization. Symbols (*) and (*) correspond to the sites of the most intense Bragg reflections expected for a) Ni_4 phase and b) NiP_2 phase

The patterns of the cobalt catalysts are different of the patterns of nickel, since it was used a different metal, which has its own characteristic peaks. Figure 19a shows the diffraction peaks at 37.0 °, 44.3 ° and 51.4 ° which are related to the cubic Co_4 phase (COD 96-900-8467). After phosphorization (Figure 19b) it is confirmed that the bonds with phosphorous differ for cobalt, a fact proven by the diffraction peaks observed at 32.2 °, 35.6 °, 46.6 °, and 48.4 °, indicating

an orthorhombic P-rich CoP phase (COD 96-900-8929) for all the three catalysts, consistent with that reported for cobalt phosphide [41]. The appearance of other minor peaks may further suggest the successful chemical conversion into CoP phases.

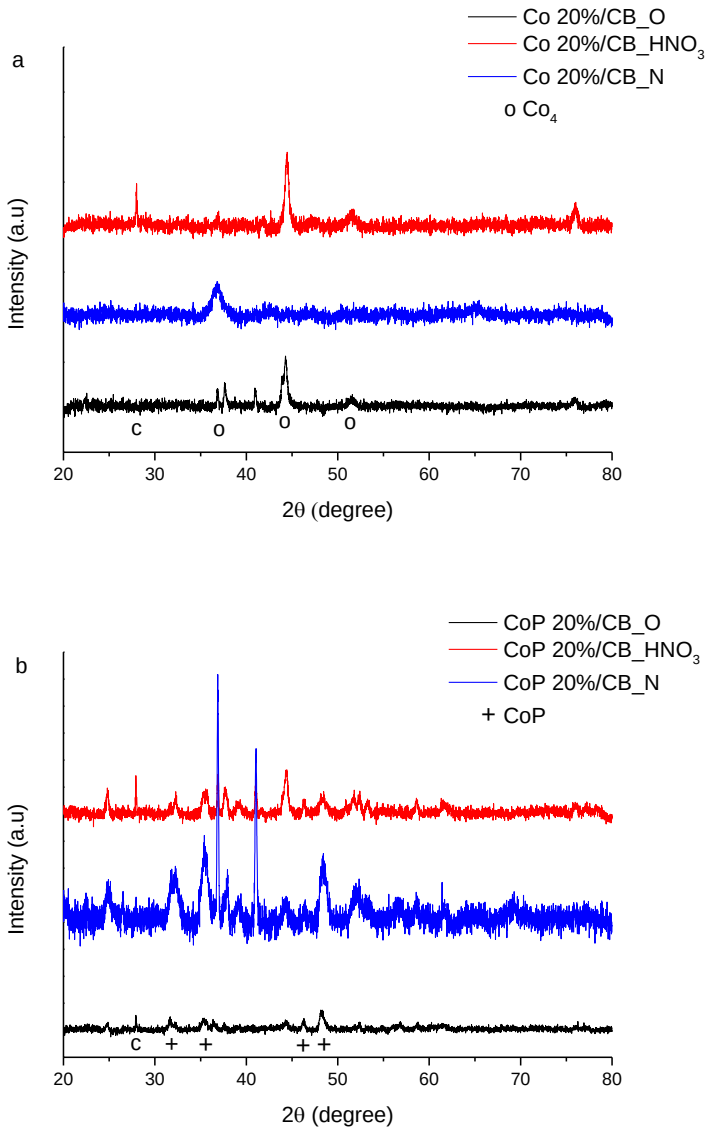

Figure 19 – XRD Patterns of Co catalysts before (a) and after (b) phosphorization. Symbols (o) and (+) correspond to the sites of the most intense Bragg reflections expected for a) Co_4 phase and b) CoP phase

For the iron catalysts, Figure 20a illustrates the diffraction peak at 44.6 ° and a small peak at 64.7 °, which indicate a characteristic cubic Fe_2 phase (COD 96-900-6589). In addition, the patterns represented in Figure 20b are consistent with that reported by Callejas *et al*. [42] for iron phosphide. Indeed, the diffraction peaks at 32.7 °, 37.2 °, 48.4 ° and 59.8 ° can suggest an orthorhombic P-rich FeP phase (COD 96-900-8933) for all the considered catalysts, further indicating that the phosphorization was, in fact, well conducted.

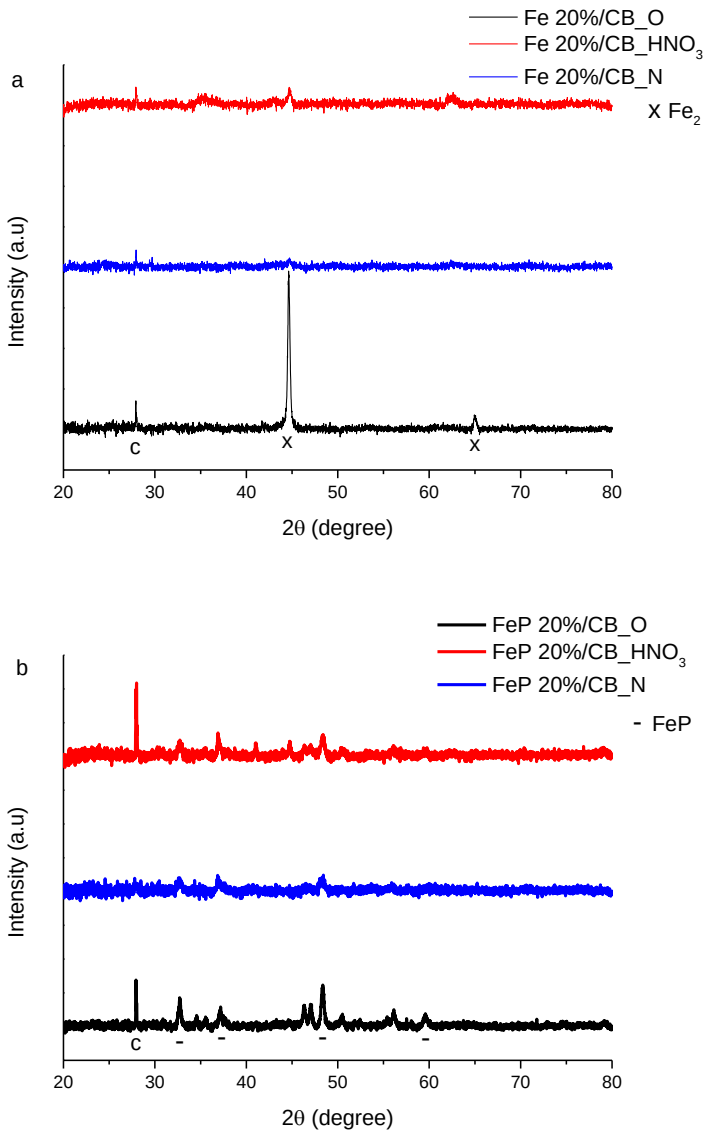

Figure 20 – XRD Patterns of Fe catalysts before (a) and after (b) phosphorization. Symbols (X) and (–) correspond to the sites of the most intense Bragg reflections expected for a) Fe_2 phase and b) FeP phase

4.4 TG

Regarding TG analysis, the thermal properties of CB_O, CB_HNO_3 and CB_N supports were studied previously to the introduction of the metals. These results are presented in Figure 21 and Table 4.

The parameters studied were the ash percentage, that is, the percentage of sample mass after combustion; the percentage of volatiles, that is, the percentage of mass loss during the heating of the samples up to 900° C in an atmosphere of N_2, and finally, the percentage of fixed carbon mass, the percentage of mass loss when changing to an atmosphere of air at 900 °C.

It can be seen that the CB_HNO_3 sample has suffered a substantial increase in the volatile matter content, which varies from 1.77% in the original CB_O to 9.00%, confirming the introduction of oxygen groups on the carbon surface, since these groups are not stable and are released with increasing temperature.

CB_N sample only suffers a modest decrease in this parameter, which is accompanied by a slight increase in ash content, further indicating the stability of the N-groups.

Table 4 – Properties measured for the different supports

Sample	*Ash (%)*	*m Volatiles (%)*	*m C_{fixed} (%)*
CB_O	7.65	1.77	90.57
CB_HNO_3	9.16	9.00	83.00
CB_N	17.2	1.45	80.93

Figure 21 shows that CB_HNO_3 starts to lose mass earlier than the CB_O sample, translating into a higher mass loss due to the increase of the volatile matter content. On the other hand, CB_N presents a lower loss of mass, confirming the stability of the N-groups.

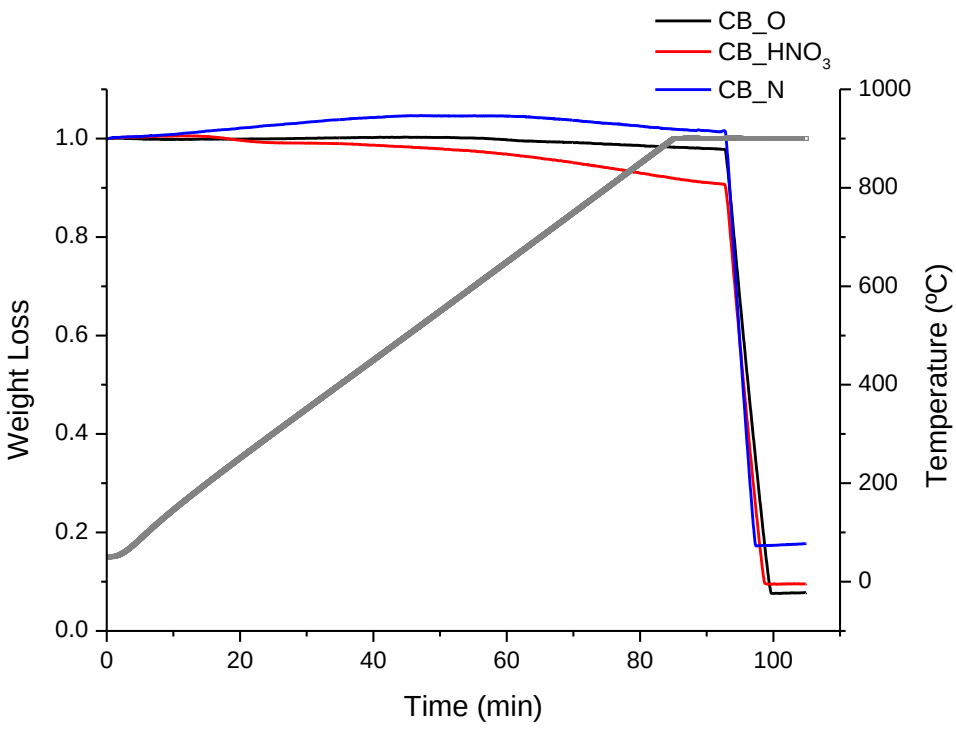

Figure 21 – TG of the different supports

The *burn-off* results and amount of metals determined after experiments in oxidative atmosphere of the metal catalysts supported in CB_O are given in Table 5. The effect of phosphorization on the CB_O supported materials corresponding to metal impregnation of 20% is also shown in Table 5.

The parameters studied were the *burn-off* percentage, that is, the material that effectively burns out, and the metal percentage, where is made an approximation of the amount of metal by subtracting the *burn-off* of the CB_O support with the *burn-off* of the considered catalyst.

Table 5 allows to infer that, general rule, as the percentage of metal increases the *burn-off* decreases, which is expected, since it is not the metal that burns out, but the support. Thus, the samples that have the highest percentage of metal, corresponding to 20%, are the ones that should undergo less burning, except for the case of Ni 15% and Ni 20%/CB_O, as well as in Co 15% and Co 20%/CB_O, despite the differences not being very significant.

Table 5 – Properties measured for the supported catalysts

Catalyst	*Burn-Off (%)*	*Metal (%)*
CB_O	92.4	-
Ni 5%/CB_O	85.2	7.2
Ni 10%/CB_O	76.9	15.5
Ni 15%/CB_O	80.4	12.0
Ni 20%/CB_O	80.2	12.2
NiP 20%/CB_O	48.3	*
Co 5%/CB_O	87.1	5.3
Co 10%/CB_O	72.6	19.8
Co 15%/CB_O	77.7	14.7
Co 20%/CB_O	76.6	15.8
CoP 20%/CB_O	50.6	*
Fe 5%/CB_O	89.1	3.3
Fe 10%/CB_O	87.0	5.4
Fe 15%/CB_O	79.1	13.3
Fe 20%/CB_O	68.9	23.5
FeP 20%/CB_O	48.9	*

The * represented in Table 5 means that the metal percentage values for the phosphorized catalysts were not included, since it was not possible to quantify the amount of metal. However, it can be assumed that they have the same metal proportion than the catalysts before phosphorization.

Furthermore, it can be seen for iron catalysts that the metal percentage is very close to the theoretical, which indicates that the deposition of the metal particles on the support was successful. In opposition, for nickel and cobalt catalysts, although the percentage obtained for 5% is close to the theoretical, the same does not occur for higher amounts of metals, and there is even a point where the metal percentage stagnates. It is important to note that this is a rough estimation, due to high analysis error. Thus, it would be necessary to carry out ICP (Inductively Coupled Plasma) analysis to truly confirm the metal content in the samples.

Regarding the phosphorized catalysts, the visualization of the TG results allows to infer that these samples only start to burn at higher temperatures and undergo less burning, therefore resulting in a lower percentage of *burn-off* (accompanied by an increase in ash content). This can be due to the phosphorous deposition along the surface of the catalyst, resulting in an increased stability. This effect is best demonstrated by the visualization of a TG result, for example of the CoP 20%/CB_O catalyst in Figure 22.

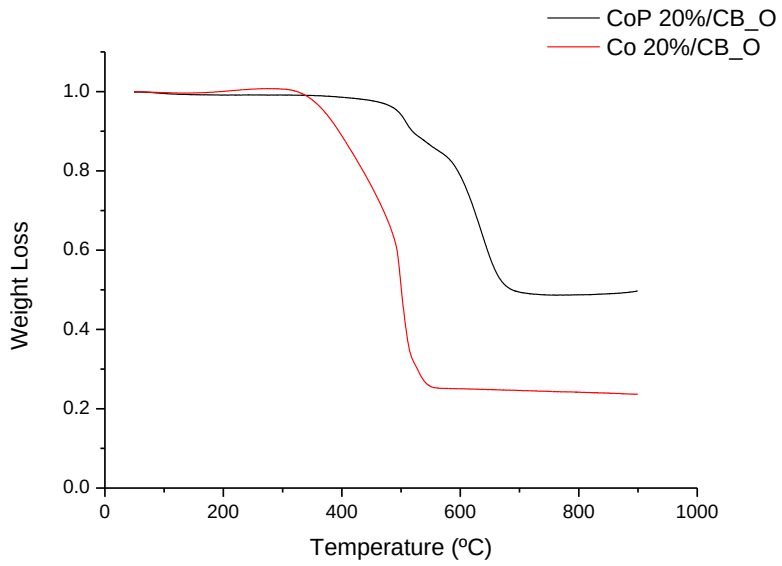

Figure 22 – TG of CoP 20% supported on CB_O

The results obtained for the impregnations corresponding to 20% for each metal supported in functionalized carbons are illustrated in Table 6.

Comparing the results obtained for the impregnation of metals in CB_O support, it can be inferred that both the introduction of oxygen groups and nitrogen groups on the carbon surface cause the material to burn at lower temperatures and less, hence the lower percentage of *burn-off* for the catalysts.

Table 6 – Properties measured for the functionalized catalysts

Catalyst	*Burn-Off (%)*
Ni 20%/CB_HNO₃	55.7
Co 20%/CB_HNO₃	58.7
Fe 20%/CB_HNO₃	64.2
Ni 20%/CB_N	66.1
Co 20%/CB_N	56.7
Fe 20%/CB_N	74.1

The results obtained for the functionalized and phosphorized samples corresponding to 20% impregnations for each metal are presented in Table 7.

Table 7 – Properties measured for the phosphorized and functionalized catalysts

Catalyst	*Burn-Off (%)*
NiP 20%/CB_HNO₃	43.4
CoP 20%/CB_HNO₃	39.3
FeP 20%/CB_HNO₃	41.6
NiP 20%/CB_N	65.5
CoP 20%/CB_N	37.8
FeP 20%/CB_N	51.8

Comparing the results obtained for the phosphorized catalysts supported in CB_O, it can be concluded that the *burn-off* decreased, except for the NiP 20%/CB_N and FeP 20%/CB_N samples. Thus, supposedly, these are the samples that undergo less burning due essentially to the combined effect of the impregnation of the metals with the introduction of functional groups and phosphorous on the carbon surface.

4.5 TPD

To further characterize the chemical surface of the carbon materials, TPD analysis were carried out. Figure 23 shows the TPD spectra for CO_2 and CO evolutions obtained of the CB_O, CB_HNO_3 and CB_N samples. In addition, Table 9 shows the amounts of CO and CO_2 released from the three supports, obtained by integration of the areas under the TPD peaks.

Table 8 - Amounts of CO and CO_2 released from the different supports

Sample	*[CO] (μmol g^{-1})*	*[CO_2] (μmol g^{-1})*
CB_O	59	395
CB_HNO₃	1064	656
CB_N	689	136

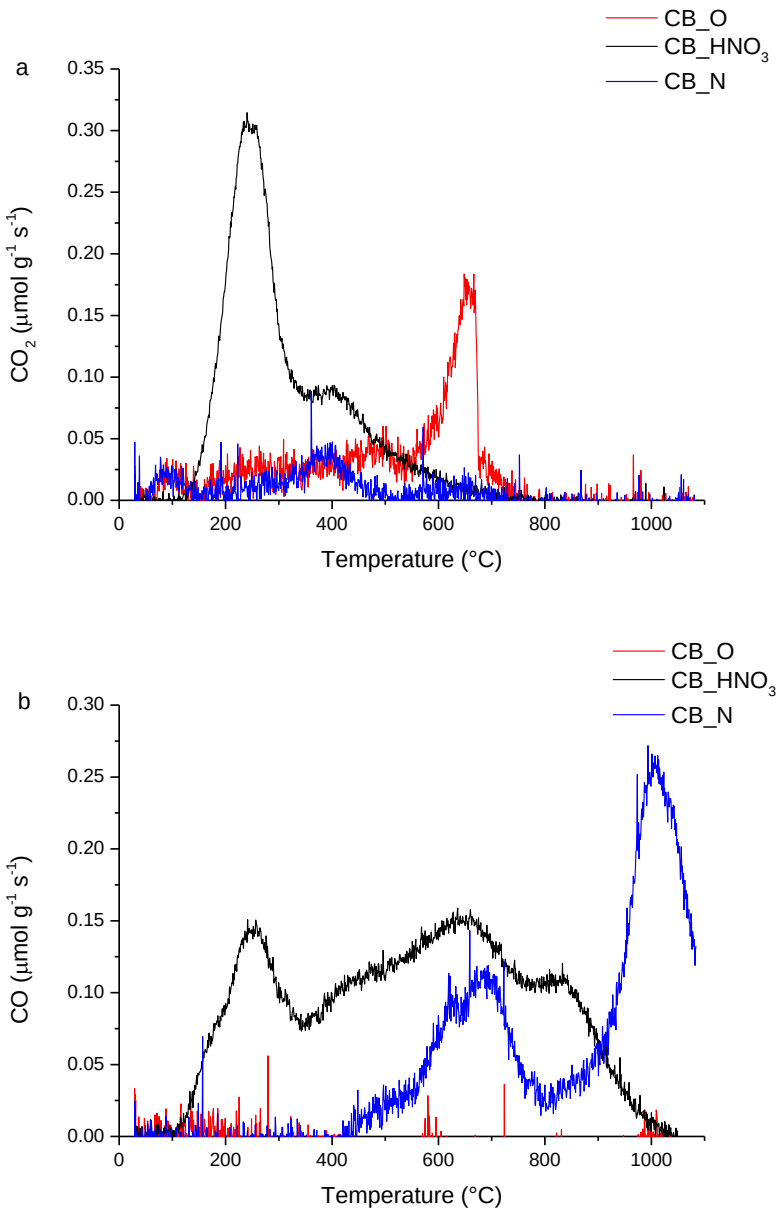

Figure 23 - TPD spectra of the different supports: a) CO_2 and b) CO evolution

An increase in the amount of oxygen surface groups is evidenced by the increase of CO and CO_2 peaks after the oxidation with nitric acid. It is important to note that the surface oxygen groups decompose by releasing CO and CO_2 in different temperature ranges.

Analysing the CO_2 evolution (Figure 23a), it can be seen that for the CB_HNO_3 support there is a release of carboxylic acid groups as CO_2 at low temperatures (150-450 ºC), as well as some anhydrides that decompose into CO_2 at intermediate temperatures (350-600 ºC). As for the CB_O sample, it is evident the release of anhydrides at the temperature range of 400-600 ºC, as well as lactones at higher temperatures (550-640 ºC). Finally, for the CB_N sample, is not observable characteristic peaks for CO_2 evolution.

Regarding CO evolution (Figure 23b), it is confirmed that the nitric acid treatment introduces large amounts of groups releasing as CO. In the case of CB_HNO_3 sample, the TPD peaks originate anhydrides (350-600 ºC), phenols at intermediate temperatures (500-750 ºC), and carbonyls/quinones that are released as CO at high temperatures (650-950 ºC). As for CB_N, the two TPD peaks suggest the decomposition of phenols at intermediate temperature range of 500-750 ºC, as well of neutral/basic groups such as carbonyls and quinones at high temperatures of 650-980 ºC. Nevertheless, since both CO and N_2 have the same molar mass (28 g mol^{-1}), it may occur some nitrogen interference in the CO signal.

4.6 Elemental Analysis

The composition of the different supports was determined by elemental analysis. The results obtained for nitrogen (N) and oxygen (O) content are presented in Table 9.

Table 9 – Elemental analysis of the different supports

Sample	*N (%)*	*O (%)*
CB_O	0.01	1.6
CB_HNO₃	0.3	7.2
CB_N	18.4	2.6

It can be seen from Table 9 that, comparing with the CB_O support, the sample CB_HNO_3 has a significant increase in oxygen content, which varies from 1.6% to 7.2%, confirming the introduction of oxygen-containing groups on the carbon surface. On the other hand, the CB_N sample has a significant increase in the amount of nitrogen, which varies from 0.01% in the CB_O sample to 18.4%, confirming the introduction of N-groups along the carbon surface. Therefore, it can be concluded that the functionalizations were well conducted.

4.7 Electrochemical Measurements

To identify the most active and promising catalysts, it was tested the electrocatalytic activity of the synthesized electrodes for HER in 0.5 M H_2SO_4 solution.

In this work, all potentials are reported versus reversible hydrogen electrode (RHE) by converting the potentials measured vs. SCE according to the following Equation 6.

$$E(RHE) = E(SCE) + 0.241 + 0.059\ pH \quad (6)$$

All linear scan voltammograms measured in the three-electrode configuration are *iR*-corrected. The correction was carried out according to the following Equation 7.

$$E_{corr} = E_{mea} - iR \times 0.85 \quad (7)$$

where E_{corr} is the *iR*-corrected potential (V), E_{mea} the experimentally measured potential (V), *i* is the current (A) flowing through the system and R is the resistance value corresponding to the highest frequency (Hz) extracted from the Nyquist plots.

The polarization curves can be obtained by plotting current density (*j*) vs. potential (V). The corrected polarization curves for the catalysts with 20% of each metal supported on the different carbon blacks, before and after phosphorization, are shown in Figures 24, 25 and 26 for Ni, Co and Fe, respectively.

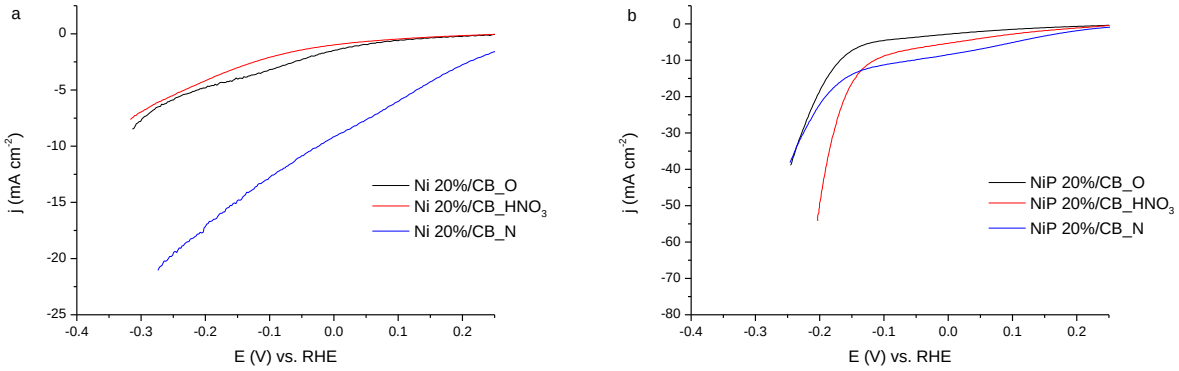

Figure 24 - Polarization curves of Ni 20% supported on the different carbon blacks before (a) and after (b) phosphorization

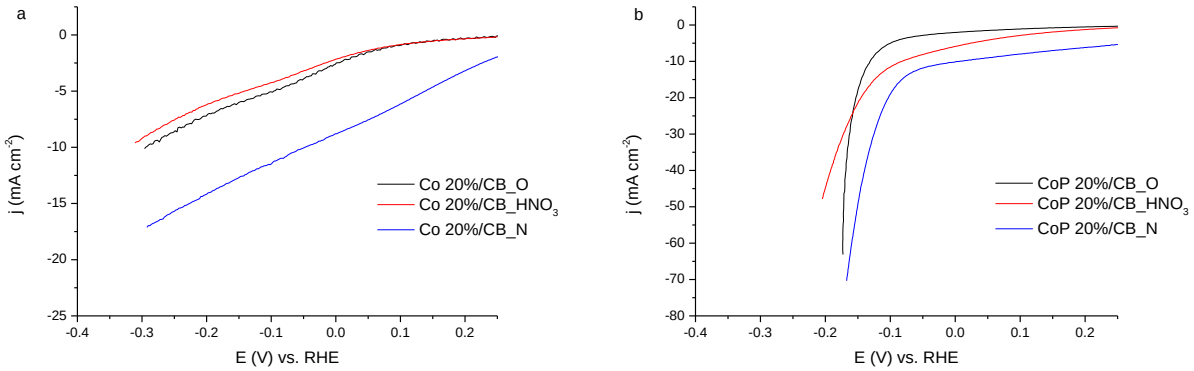

Figure 25 - Polarization curves of Co 20% supported on the different carbon blacks before (a) and after (b) phosphorization

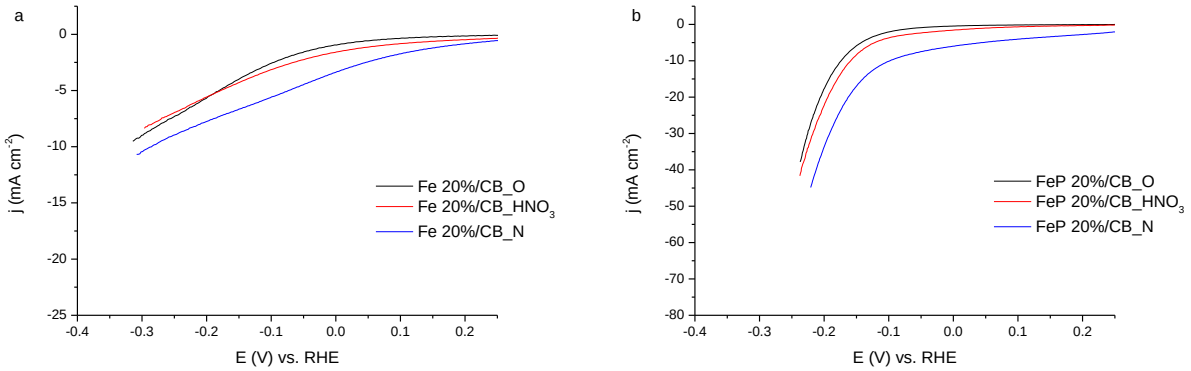

Figure 26 - Polarization curves of Fe 20% supported on the different carbon blacks before (a) and after (b) phosphorization

Observing the figures it can be concluded that the introduction of oxygen-containing groups does not influence significantly the catalytic activity of the materials. In fact, taking into account the textural properties measured for the different supports, it was reported that the treatment with nitric acid may have originated some damage on the graphitic surface, therefore leading to the deterioration of the structure and electrical properties of carbon black.

On the other hand, the N-doped samples present better results. In Figure 25 it can be verified that there is a slight increase of the catalytic activity when higher values of current density (*j*) are reached. This effect can be due to the introduction of N-groups on the carbon surface, creating nitrogenated sites that are more chemically active for HER. These sites modify and enhance the carbon properties, such as the electrical conductivity, basicity, oxidation stability and catalytic activity, as reported in the literature [50]. In addition, the catalysts supported in CB_N are the ones with larger BET surface areas (see Table 3), which may increase the catalytic activity.

Regarding TEM images, it was found that after N-doping with melamine the surface morphology of the catalysts became more rough and disordered. In fact, according to Chen *et al*. [54], the disruptions and irregular curvatures in graphene stacking in CB_N could be due to the propensity of incorporated nitrogen to form pentagonal and hexagonal defects in the graphene layers. So, it appears that the introduction of such defects disrupts the planar hexagonal arrangement of carbon atoms in CB and results in an increased catalytic activity for HER.

When comparing the results obtained before and after phosphorization, it is noted that this procedure plays an important role in the significant increase of the catalytic activity as well as in the stability of the materials. In fact, according to Zhang *et al*. [55], P atoms with more electronegativity can draw electrons from metal atoms and so, the negatively charged P can act as base to trap positively charged proton during electrochemical HER.

Also, with appropriate difference in electronegativity and atomic ratio of metal and P, transition metal phosphides are able to exhibit a metallic character and an increase in conductivity, especially for the metal-rich phosphides. In addition, corrosion resistance of transition metal phosphides in acidic media is directly correlated with P content, as reported by Kucernak *et al*. [39]. However, with the P content increasing, P atoms can greatly restrict the electron delocalization of the metal atoms, and therefore imped the conductivity, resulting in a weakened HER activity [55]. From this it is possible to conclude that is necessary to optimize the amount of phosphorous present on the electrocatalysts.

On the other hand, and according to XRD results, the existence of different crystalline phases on the catalysts also seem to have influence on the results obtained. In fact, the P-rich CoP phase appears to be the more active phase for HER. The reason behind the catalysts impregnated with cobalt present the best electrochemical results can be due to its atomic arrangement that presents greater affinity with the P atoms, in comparison to those of nickel and iron. Therefore, Co and P can tune each other's electronic properties to produce a more active catalyst phase.

From the obtained results it is possible to conclude that the most promising materials to catalyse HER are CoP 20%/CB_O and CoP 20%/CB_N. For comparison, Figure 27 shows the corrected polarization curves for commercial Pt/C (20 wt.%) catalyst, CoP 20%/CB_O and CoP 20%/CB_N.

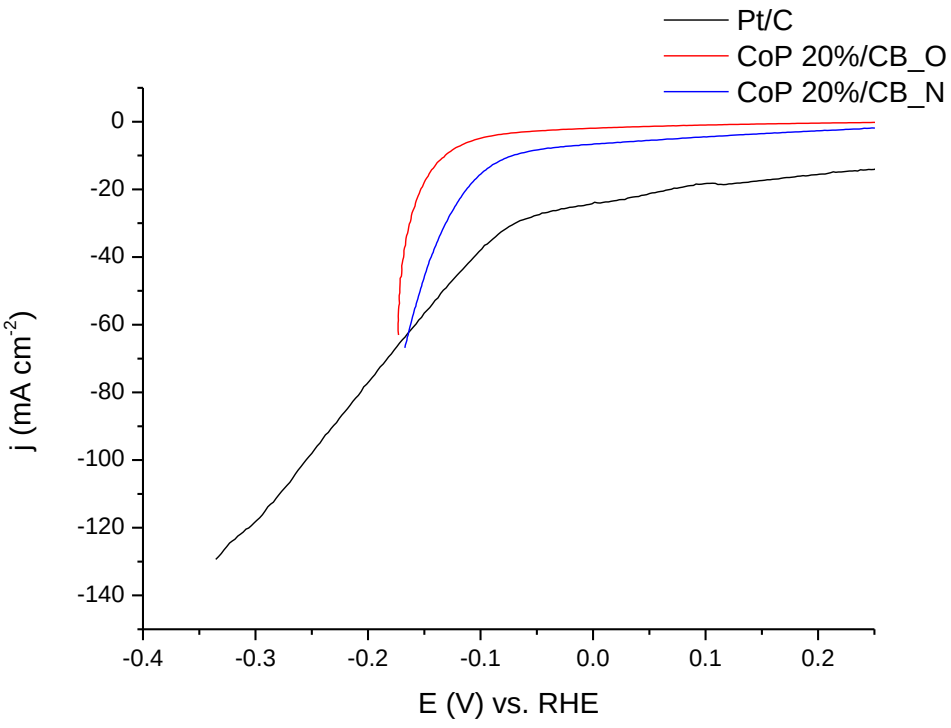

Figure 27 - Polarization curves of Pt/C, CoP 20%/CB_O and CoP 20%/CB_N

The polarization curve allows to infer that the commercial Pt/C exhibits a significantly higher catalytic activity for HER than the TMP's selected, since it was achieved the highest value of current density, approximately 135 mA cm^{-2}.

Replotting the polarization curves into Tafel plots (overpotential vs. log [j]), the Tafel slope can be determined by fitting the linear regions of Tafel plots to the Tafel Equation 8.

$$\eta = b \times \log (j/j_0) \quad (8)$$

where η is the overpotential (V), b is the Tafel slope (mV dec^{-1}), j is the current density (mA cm^{-2}), and j_0 is the exchange current density (mA cm^{-2}).

So, to better compare the most promising catalysts, key kinetic parameters such as Tafel slope, as well as η_{10}, η_{20} and η_{50} were then determined and can be shown in Table 10.

Table 10 – Kinetic parameters of the catalysts

Catalyst	η_{10} *(mV)*	η_{20} *(mV)*	η_{50} *(mV)*	*Tafel Slope (mV* dec^{-1}*)*
CoP 20%/CB_O	-132	-153	-169	77
CoP 20%/CB_N	-71	-113	-154	122

The CoP 20%/CB_O electrode needs overpotentials of -132 (η_{10}), -153 (η_{20}) and -169 mV (η_{50}) to drive HER at current densities of 10, 20 and 50 mA cm^{-2}, respectively. In contrast, the CoP 20%/CB_N electrode presents a higher performance with lower overpotentials of -71 (η_{10}), -113 (η_{20}) and -154 mV (η_{50}), requiring less energy to achieve the same current density.

Regarding Tafel slope, the smaller its value means that increasing the same current density requires smaller overpotential, implying a faster charge transfer kinetic. As previously indicated, under acidic conditions, HER undergoes by a multistep reaction process, which is suggested as two different mechanisms with three possible reactions. The dominant reaction mechanism in the HER process can be theoretically indicated by the Tafel slope.

The CoP 20%/CB_O catalyst exhibited a Tafel slope of 77 mV dec^{-1}, larger than that reported for Pt/C (30 mV dec^{-1}) [41], but surprisingly superior to that of CoP 20%/CB_N (122 mV dec^{-1}). The Tafel slopes obtained for the synthesized catalysts are slightly larger from the values reported in the literature for many earth-abundant HER catalysts reported recently, such as Ni_2P NP's (46 mV dec^{-1}) [38], CoP/CNT (54 mV dec^{-1}) [41] and FeP/Ti (37 mV dec^{-1}) [42], however, the difference is not very high, indicating that, with some improvements, TMP's could be capable of replacing PGM's.

The obtained slope values suggest that the HER taking place on the CoP 20%/CB_O and CoP 20%_CB_N catalyst surfaces would follow a Volmer–Heyrovsky mechanism, and that the rate of the discharge step would be consistent with that of the desorption step.

In order to further study the stability of the materials after prolonged operation in acidic environment, it was carried out Chronopotentiometry experiments for the most promising catalysts and also for Pt, performed at a fixed cathodic current density of 20 mA cm^{-2} for approximately 12 h. Figure 28 shows that the transition metal phosphide electrodes exhibit good long-term durability in acidic media, since the overpotential only increased from 111 to 114 mV in case of CoP 20%/CB_O and from 115 to 116 mV for CoP 20%/CB_N, further indicating the stability of N-groups. Surprisingly, for Pt it seems that there is an initial period of stabilization and then the overpotential increases from 115 to 118 mV during the estimated time. So, compared with Pt, the transition metal phosphide catalysts demonstrate to have admirable stability after prolonged operation.

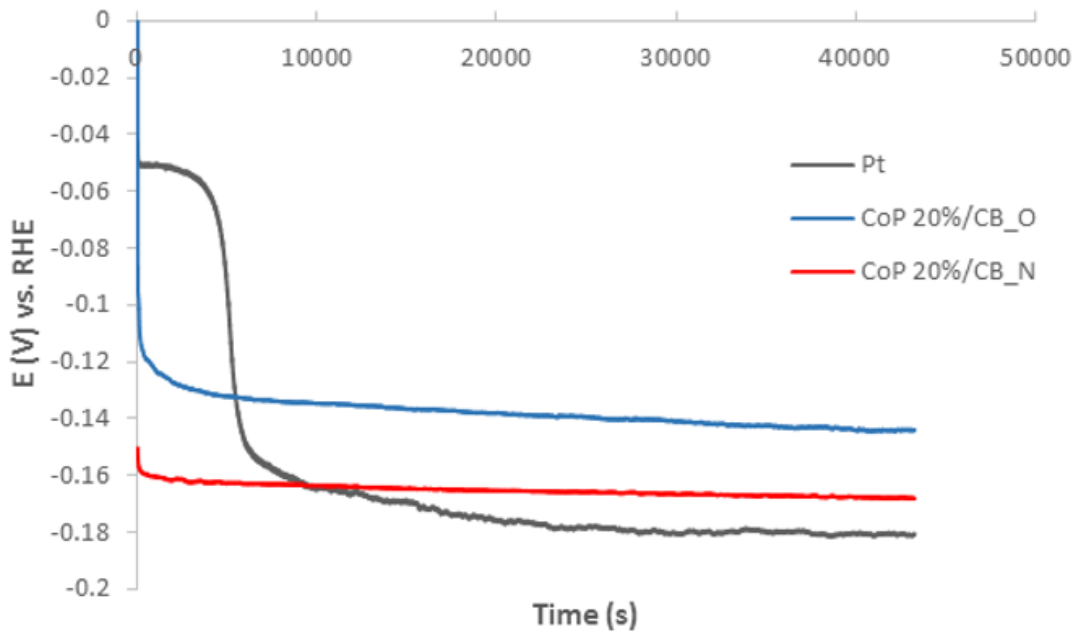

Figure 28 – Chronopotentiometric curves recorded at −20 mA cm^{-2} for Pt, CoP 20%/CB_O and CoP 20%/CB_N

5 Conclusions

It was assessed the influence of support chemistry and the presence of phosphides, which showed to be beneficial regarding the electrochemical results, to significantly increase the catalytic activity as well as the stability of the synthesized catalysts.

The characterization results confirm that the functionalizations with oxygen and nitrogen containing groups were achieved. Self-supported electrodes integrated with TMP's electrocatalysts were fabricated by immobilization of the NP's on functionalized carbon paper, followed by a suitable one-step phosphorization treatment. The as-fabricated electrodes exhibited good electrocatalytic performance towards HER with emphasis on the samples of CoP 20%/CB_O and CoP 20%/CB_N with Tafel slopes of 77 and 122 mV dec^{-1}, respectively, larger than that reported for Pt/C, but still acceptable. The slopes suggest that the HER takes place on the electrode's surface following a Volmer–Heyrovsky mechanism, and that the rate of the discharge step would be consistent with that of the desorption step. The durability test performed at a fixed cathodic current density of 20 mA cm^{-2} for approximately 12 h shows that the overpotential only increased from 111 to 114 mV in the case of CoP 20%/CB_O and from 115 to 116 mV for CoP 20%/CB_N, demonstrating good long-term stability of the electrodes in acidic medium.

The N-doped samples present better results, which is due to the introduction of N-groups on the carbon surface, modifying and enhancing the carbon properties, such as the electrical conductivity, basicity, oxidation stability and catalytic activity. In addition, as indicated by the textural properties, the catalysts supported in CB_N are the ones with larger BET surface areas, which may be related to the increase of the catalytic activity. It was confirmed that phosphorization plays an important role in the significant increase of the catalytic activity for HER, as well as in the stability of materials. Furthermore, the existence of different crystalline phases of the catalysts has influence on the results obtained, in which the P-rich CoP phase appears to be the more active phase for HER. Therefore, Co and P seem to properly tune each other's electronic properties to produce a more active catalyst.

In conclusion, this work provides a general strategy for the synthesis of electrocatalysts based on carbon materials decorated with transition metal phosphides for HER applications, which should be further investigated, since it is proven that the TMP's, with the necessary improvements, have indeed the potential to replace Pt in the long term.

6 Assessment of the work done

6.1 Objectives Achieved

The main goal of this dissertation was to explore the electrocatalytic properties of phosphide NP's of Ni, Co and Fe supported in carbon black. Appropriate and robust functional characterization of the electrocatalysts developed was carried out by a set of techniques such as N_2 isotherms, TEM, XRD, TG, TPD, EA, as well as electrochemical measurements such as LSV in order to evaluate their activity and stability. Thus, the main objective of this dissertation was fulfilled.

6.2 Limitations and Future Work

As main limitation I refer the lack of time, since it would be possible to have tested alternative synthesis procedures, more performance tests to further characterize electrochemically the catalysts, different loadings, different percentages of metal, as well as the determination of the active area of the catalysts.

As future work it would be interesting to incorporate the most promising HER PGM-free catalysts into MEA's for testing in PEM water electrolysis prototypes. The performance of the *single cell* should be investigated in terms of activity (hydrogen and oxygen production rates) and durability under steady-state polarization and startup-shutdown cycles. Also, it could be tested different catalyst loadings on the working electrode in order to see the differences in the respective electrocatalytic activities. Finally, and to improve further the catalytic performances of phosphides, it could be prepared ternary phosphides in order to verify a possible synergistic effect between two metals in these phosphides.

6.3 Final Assessment

My appreciation of the work done is very positive. I consider that I have achieved the main goal proposed and I have confidence in the results obtained. I also believe that this investigation project has a lot more to explore and develop, so I would like very much to have the opportunity to do so.

References

[1] Carvalho, M., *Preparação e caraterização de elétrodos de óxido níquel para eletrolisadores alcalinos de produção de hidrogénio*, in *Tecnologia e Valorização Ambiental e Produção de Energia*. 2013, Escola Superior de Tecnologia e Gestão: Instituto Politécnico de Portalegre.

[2] Hidrogénio, A.P.p.a.P.d. *Desafios e Oportunidades da Economia do Hidrogénio*. 2008.

[3] Badwal, S.P., Giddey, S.S., Munnings, C., Bhatt, A.I.Hollenkamp, A.F., *Emerging electrochemical energy conversion and storage technologies*. Frontiers in Chemistry, 2014. **2**: p. 79.

[4] Ursua, A., Gandia, L.M.Sanchis, P., *Hydrogen Production From Water Electrolysis: Current Status and Future Trends*. Proceedings of the IEEE, 2012. **100**(2): p. 410.

[5] *High-efficiency, low-cost catalyst for water electrolysis*. (2018). Retrieved from https://phys.org/news/2018-02-high-efficiency-low-cost-catalyst-electrolysis.html

[6] Rashid, M.M., *Hydrogen Production by Water Electrolysis: A Review of Alkaline Water Electrolysis, PEM Water Electrolysis and High Temperature Water Electrolysis*. International Journal of Engineering and Advanced Technology, 2015. **4**(3): p. 80.

[7] Langemann, M., Fritz, D.L., Müller, M.Stolten, D., *Validation and characterization of suitable materials for bipolar plates in PEM water electrolysis*. International Journal of Hydrogen Energy, 2015. **40**(35): p. 11385.

[8] Millet, P., Ngameni, R., Grigoriev, S.A., Mbemba, N., Brisset, F., Ranjbari, A.Etiévant, C., *PEM water electrolyzers: From electrocatalysis to stack development*. International Journal of Hydrogen Energy, 2010. **35**(10): p. 5043.

[9] Vincent, I.Bessarabov, D., *Low cost hydrogen production by anion exchange membrane electrolysis: A review*. Renewable and Sustainable Energy Reviews, 2018. **81**: p. 1690.

[10] Carmo, M., Fritz, D.L., Mergel, J.Stolten, D., *A comprehensive review on PEM water electrolysis*. International Journal of Hydrogen Energy, 2013. **38**(12): p. 4901.

[11] Lipman, T., *An Overview of Hydrogen Production and Storage Systems with Renewable Hydrogen Case Studies*. Clean Energy States Alliance, 2011.

[12] Wang, X., Li, W., Xiong, D., Petrovykh, D.Y.Liu, L., *Bifunctional Nickel Phosphide Nanocatalysts Supported on Carbon Fiber Paper for Highly Efficient and Stable Overall Water Splitting*. Advanced Functional Materials, 2016. **26**(23): p. 4067.

[13] Costa, J.D., Lado, J.L., Carbó-Argibay, E., Paz, E., Gallo, J., Cerqueira, M.F., Rodríguez-Abreu, C., Kovnir, K.Kolen'ko, Y.V., *Electrocatalytic Performance and Stability of Nanostructured Fe-Ni Pyrite-Type Diphosphide Catalyst Supported on Carbon Paper*. The Journal of Physical Chemistry C, 2016. **120**(30): p. 16537.

[14] Lin, Y., Zhang, J., Pan, Y.Liu, Y., *Nickel phosphide nanoparticles decorated nitrogen and phosphorus co-doped porous carbon as efficient hybrid catalyst for hydrogen evolution*. Applied Surface Science, 2017. **422**: p. 828.

[15] Pan, Y., Yang, N., Chen, Y., Lin, Y., Li, Y., Liu, Y.Liu, C., *Nickel phosphide nanoparticles-nitrogen-doped graphene hybrid as an efficient catalyst for enhanced hydrogen evolution activity*. Journal of Power Sources, 2015. **297**: p. 45.

[16] Zhou, W., Jia, J., Lu, J., Yang, L., Hou, D., Li, G.Chen, S., *Recent developments of carbon-based electrocatalysts for hydrogen evolution reaction.* Nano Energy, 2016. **28**: p. 29.

[17] Sathe, B.R., Zou, X.Asefa, T., *Metal-free B-doped graphene with efficient electrocatalytic activity for hydrogen evolution reaction.* Catalysis, Science & Technology, 2014. **4**(7): p. 2023.

[18] Suryanto, B.H.Zhao, C., *Surface-oxidized carbon black as a catalyst for the water oxidation and alcohol oxidation reactions.* Chemical Communications, 2016. **52**(38): p. 6439.

[19] Zou, X.Zhang, Y., *Noble metal-free hydrogen evolution catalysts for water splitting.* Chemical Society Reviews, 2015. **44**(15): p. 5148.

[20] Li, Y., Wang, H., Xie, L., Liang, Y., Hong, G.Dai, H., *MoS2 nanoparticles grown on graphene: an advanced catalyst for the hydrogen evolution reaction.* Journal of the American Chemical Society, 2011. **133**(19): p. 7296.

[21] Abbas, M.A.Bang, J.H., *Rising Again: Opportunities and Challenges for Platinum-Free Electrocatalysts.* Chemistry of Materials, 2015. **27**(21): p. 7218.

[22] Tahir, M., Pan, L., Idrees, F., Zhang, X., Wang, L., Zou, J.-J.Wang, Z.L., *Electrocatalytic oxygen evolution reaction for energy conversion and storage: A comprehensive review.* Nano Energy, 2017. **37**: p. 136.

[23] Cheng, Y.Jiang, S.P., *Advances in electrocatalysts for oxygen evolution reaction of water electrolysis-from metal oxides to carbon nanotubes.* Progress in Natural Science: Materials International, 2015. **25**(6): p. 545.

[24] Pan, Y., Liu, Y.Liu, C., *Nanostructured nickel phosphide supported on carbon nanospheres: Synthesis and application as an efficient electrocatalyst for hydrogen evolution.* Journal of Power Sources, 2015. **285**: p. 169.

[25] Ma, C.B., Qi, X., Chen, B., Bao, S., Yin, Z., Wu, X.J., Luo, Z., Wei, J., Zhang, H.L.Zhang, H., *MoS2 nanoflower-decorated reduced graphene oxide paper for high-performance hydrogen evolution reaction.* Nanoscale, 2014. **6**(11): p. 5624.

[26] Tang, H., Dou, K., Kaun, C.-C., Kuang, Q.Yang, S., *MoSe2nanosheets and their graphene hybrids: synthesis, characterization and hydrogen evolution reaction studies.* Journal of Materials Chemistry A, 2014. **2**(2): p. 360.

[27] Zhang, Z., Lu, B., Hao, J., Yang, W.Tang, J., *FeP nanoparticles grown on graphene sheets as highly active non-precious-metal electrocatalysts for hydrogen evolution reaction.* Chemical Communications, 2014. **50**(78): p. 11554.

[28] Pan, Y., Hu, W., Liu, D., Liu, Y.Liu, C., *Carbon nanotubes decorated with nickel phosphide nanoparticles as efficient nanohybrid electrocatalysts for the hydrogen evolution reaction.* Journal of Materials Chemistry A, 2015. **3**(24): p. 13087.

[29] Rodriguez, J.A., *Catalysts for Hydrogen Evolution from the [NiFe] Hydrogenase to the Ni2P(001) Surface: The Importance of Ensemble Effect.* Journal of the American Chemical Society, 2005. **127**: p. 14871.

[30] Prins, R.Bussell, M.E., *Metal Phosphides: Preparation, Characterization and Catalytic Reactivity.* Catalysis Letters, 2012. **142**(12): p. 1413.

[31] Zhao, H.Yuan, Z.-Y., *Transition metal-phosphorus-based materials for electrocatalytic energy conversion reactions.* Catalysis Science & Technology, 2017. **7**(2): p. 330.

[32] Oyama, S.T., Gott, T., Zhao, H.Lee, Y.-K., *Transition metal phosphide hydroprocessing catalysts: A review*. Catalysis Today, 2009. **143**(1-2): p. 94.

[33] Callejas, J.F., Read, C.G., Roske, C.W., Lewis, N.S.Schaak, R.E., *Synthesis, Characterization, and Properties of Metal Phosphide Catalysts for the Hydrogen-Evolution Reaction*. Chemistry of Materials, 2016. **28**(17): p. 6017.

[34] Kanatzidis, M.G., Pottgen, R.Jeitschko, W., *The metal flux: a preparative tool for the exploration of intermetallic compounds*. Angewandt Chemie, 2005. **44**(43): p. 6996.

[35] Abu, I.Smith, K., *The effect of cobalt addition to bulk MoP and Ni2P catalysts for the hydrodesulfurization of 4,6-dimethyldibenzothiophene*. Journal of Catalysis, 2006. **241**(2): p. 356.

[36] Yang, X., Lu, A.-Y., Zhu, Y., Hedhili, M.N., Min, S., Huang, K.-W., Han, Y.Li, L.-J., *CoP nanosheet assembly grown on carbon cloth: A highly efficient electrocatalyst for hydrogen generation*. Nano Energy, 2015. **15**: p. 634.

[37] Wang, D.Astruc, D., *The recent development of efficient Earth-abundant transition-metal nanocatalysts*. Chemical Society Reviews, 2017. **46**(3): p. 816.

[38] Popczun, E.J., McKone, J.R., Read, C.G., Biacchi, A.J., Wiltrout, A.M., Lewis, N.S.Schaak, R.E., *Nanostructured nickel phosphide as an electrocatalyst for the hydrogen evolution reaction*. Journal of the American Chemical Society, 2013. **135**(25): p. 9267.

[39] Kucernak, A.R.J.Naranammalpuram Sundaram, V.N., *Nickel phosphide: the effect of phosphorus content on hydrogen evolution activity and corrosion resistance in acidic medium*. Journal of Materials Chemistry A, 2014. **2**(41): p. 17435.

[40] Feng, L.Xue, H., *Advances in Transition-Metal Phosphide Applications in Electrochemical Energy Storage and Catalysis*. ChemElectroChem, 2017. **4**(1): p. 20.

[41] Liu, Q., Tian, J., Cui, W., Jiang, P., Cheng, N., Asiri, A.M.Sun, X., *Carbon nanotubes decorated with CoP nanocrystals: a highly active non-noble-metal nanohybrid electrocatalyst for hydrogen evolution*. Angewandt Chemie, 2014. **53**(26): p. 6710.

[42] Callejas, J.F., *Electrocatalytic and Photocatalytic Hydrogen Production from Acidic and Neutral-pH Aqueous Solutions Using Iron Phosphide Nanoparticles*. American Chemical Society, 2014.

[43] Serp, P., *Carbon nanotubes and nanofibers in catalysis*. Applied Catalysis A: General, 2003. **253**(2): p. 337.

[44] Sairanen, E., *Modification of carbon materials for catalyst applications*, in *Department of Biotechnology and Chemical Technology*. 2015, Aalto University School of Chemical Technology.

[45] Machado, P.S.a.B., *Carbon (Nano)materials for Catalysis*, in *Nanostructured Carbon Materials for Catalysis*, Royal Society of Chemistry, Editor. 2015. p. 1.

[46] Figueiredo, J.L., *Functionalization of porous carbons for catalytic applications*. Journal of Materials Chemistry A, 2013. **1**(33).

[47] Figueiredo, J.L.Pereira, M.F.R., *The role of surface chemistry in catalysis with carbons*. Catalysis Today, 2010. **150**(1-2): p. 2.

[48] Boehm, H.P., *SOME ASPECTS OF THE SURFACE CHEMISTRY OF CARBON BLACKS AND OTHER CARBON*. Elsevier Science, 1994. **32**(5): p. 759.

[49] J.L. Figueiredo, M.F.R.P., M.M.A. Freitas, J.J.M. Órfão, *Modification of the surface chemistry of activated carbons*. Elsevier Science, 1999: p. 1379.

[50] Duarte, M.F.P., *Nova geração de materiais de elétrodo para aplicação em células de combustível*, in *Departamento de Engenharia Química*. 2016, Faculdade de Engenharia da Universidade do Porto.

[51] Vieira, R., Pham-Huu, C., Keller, N.Ledoux, M.J., *New carbon nanofiber/graphite felt composite for use as a catalyst support for hydrazine catalytic decomposition*. Chemical Communications, 2002(9): p. 954.

[52] Soares, O.S.G.P., Órfão, J.J.M.Pereira, M.F.R., *Nitrate Reduction Catalyzed by Pd-Cu and Pt-Cu Supported on Different Carbon Materials*. Catalysis Letters, 2010. **139**(3-4): p. 97.

[53] Soares, O.S.G.P., Rocha, R.P., Gonçalves, A.G., Figueiredo, J.L., Órfão, J.J.M.Pereira, M.F.R., *Easy method to prepare N-doped carbon nanotubes by ball milling*. Carbon, 2015. **91**: p. 114.

[54] Chen, Y., Wang, J., Liu, H., Banis, M.N., Li, R., Sun, X., Sham, T.-K., Ye, S.Knights, S., *Nitrogen Doping Effects on Carbon Nanotubes and the Origin of the Enhanced Electrocatalytic Activity of Supported Pt for Proton-Exchange Membrane Fuel Cells*. The Journal of Physical Chemistry C, 2011. **115**(9): p. 3769.

[55] Shi, Y. Zhang, B., *Recent advances in transition metal phosphide nanomaterials: synthesis and applications in hydrogen evolution reaction*. Chemical Society Reviews, 2016. **45**(6): p. 1529.

Appendix 1 Experimental Installations

In this Appendix are presented photographs of the equipments that were used in the course of the present work.

Figure 29 - Ovens from the Laboratory of Catalysis and Materials in FEUP used for the reduction of materials in hydrogen

Figure 30 - NOVA 4200e equipment from Quantachrome Instruments of the Laboratory of Catalysis and Materials in FEUP

Figure 31 – TG equipment of the Laboratory of Catalysis and Materials in FEUP

Figure 32 - AMI-300 equipment from Altamira Instruments from the Laboratory of Catalysis and Materials in FEUP

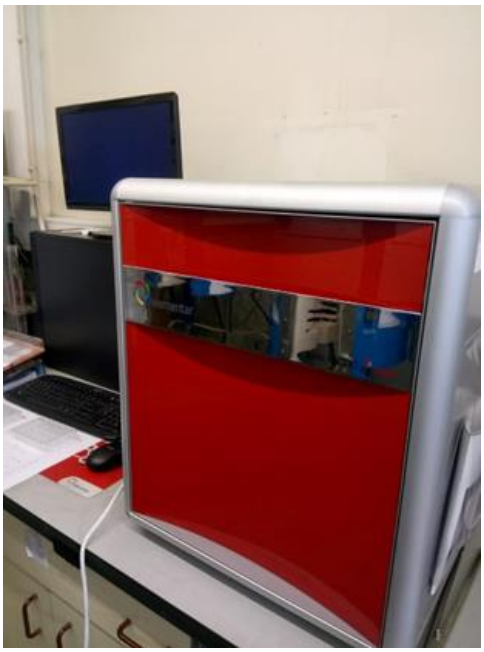

Figure 33 - MICRO cube analyzer from Elemental GmbH in CHNS mode from Laboratory of Catalysis and Materials in FEUP

Figure 34 - OXY cube analyzer from Elemental GmbH from Laboratory of Catalysis and Materials in FEUP

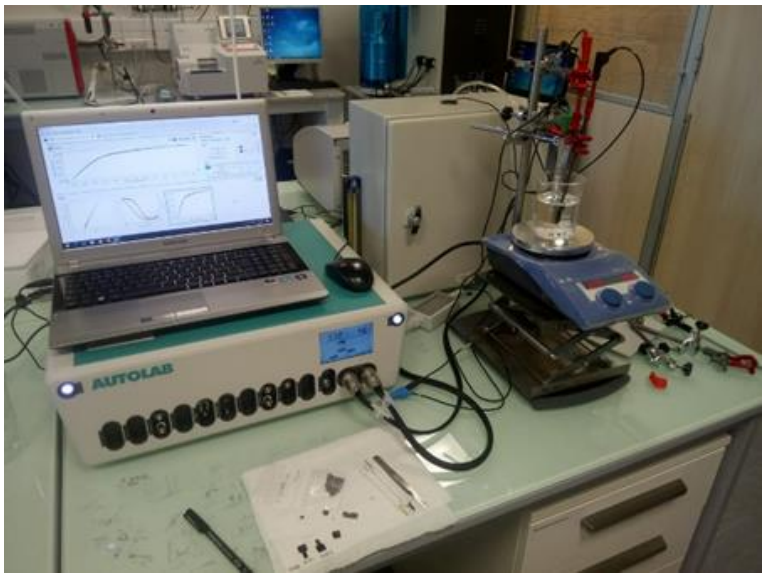

Figure 35 - Metrohm Autolab PGSTAT302N potentiostat/galvanostat used in INL